



ORIGINAL ARTICLE

Experimental and theoretical approach for novel imidazolium ionic liquids as Smart Corrosion inhibitors for mild steel in 1.0 M hydrochloric acid



A. Nahlé^{a,*}, R. Salim^b, F. EL Hajjaji^b, E. Ech-chihbi^b, A. Titi^c, M. Messali^d, S. Kaya^e, B. El IBrahimi^f, M. Taleb^b

^a Department of Chemistry, College of Sciences, University of Sharjah, Sharjah, P.O. Box: 27272, United Arab Emirates

^b Engineering Laboratory of Organometallic, Molecular Materials, and Environment, Faculty of Sciences, University Sidi Mohamed Ben Abdellah, Fez, Morocco

^c Laboratory of Applied and Environmental Chemistry (LCAE), Mohammed first University, Oujda, Morocco

^d Chemistry Department, Faculty of Science, Taibah University, 30002 Al-Madinah Al-Mounawwara, Saudi Arabia

^e Sivas Cumhuriyet University, Health Services Vocational School, Department of Pharmacy, 58140 Sivas, Turkey

^f Department of Applied Chemistry, Faculty of Applied Sciences, 86153 Ait Melloul, IBN ZOHR University, Morocco

Received 12 February 2022; accepted 16 May 2022

Available online 20 May 2022

KEYWORDS

Ionic liquids;
Inhibition performance;
Adsorption;
DFT method;
Mild steel, molecular
dynamic simulation

Abstract 3-(4-hydroxybutyl)-1-phenethyl-1H-imidazol-3-ium chloride ([HB-Imid] Cl), and 3-(2-chlorobenzyl)-1-phenethyl-1H-imidazol-3-ium chloride ([CB-Imid] Cl) were investigated as corrosion inhibitors for mild steel in 1.0 M hydrochloric acid solution. Electrochemical techniques (PDP and EIS) were performed as experimental studies while DFT at B3LYP 6-311G (df,pd), and molecular dynamic simulation were used as theoretical approach. PDP experiments revealed that the studied ionic liquids (ILs) behaved as mixture type inhibitors. EIS results indicated that these compounds showed good inhibition performance with inhibition efficiency around 95% at the optimum concentration of 1.0×10^{-3} M. According to Langmuir isotherm model and the thermodynamic parameters, these ILs were adsorbed onto the mild steel surface through physical and chemical bonds. SEM and EDX examinations proved the formation of a protective layer of adsorbed inhibitors at the steel surface. The DFT/B3LYP/6-311G(df,pd) computations in both the gas and water environments disclosed that [HB-Imid] Cl molecule was softer and had a lower energy gap, electrodonating power, and polarizability indexes.

© 2022 The Author(s). Published by Elsevier B.V. on behalf of King Saud University. This is an open access article under the CC BY-NC-ND license (<http://creativecommons.org/licenses/by-nc-nd/4.0/>).

* Corresponding author.

E-mail address: anahle@sharjah.ac.ae (A. Nahlé).

Peer review under responsibility of King Saud University.

1. Introduction

Numerous industrial processes such as pipeline construction for gas and oil transport, acid descaling, and acid pickling are using mild steel as construction materials because of its



Production and hosting by Elsevier

high availability and physicochemical characteristics besides its low cost (Mohagheghi and Arefinia, 2018; Nkuna et al., 2020).

On the other hand, this material can be easily damaged leading to economic and human disasters when it is cleaned and descaled with an aggressive acidic medium especially hydrochloric acid (1.0 M). Thus, this phenomenon is a serious problem that takes the attention of many researchers. Therefore, corrosion inhibitors are one of the mainly significant methods for metal protection commonly employed at low concentrations in acidic solutions which minimize the corrosive attack on metallic materials (Vinutha and Venkatesha, 2016; Salim et al., 2019). These inhibitors can adsorb on the mild steel surface in form of a barrier film. This film can be formed by several active sites in the inhibitor's structure such as heteroatoms' centers "N, S, and O", and π -electrons of multiple (double and triple) bonds and aromatic rings. This film is formed through either physical, chemical, or both physical and chemical adsorption (Bouoidina et al., 2020).

Many researchers pay attention to the application of eco-friendly corrosion inhibitors such as pharmaceutical products (Mrani et al., 2018), natural extracts (Marsoul et al., 2020), ionic liquids (ILs), etc. Recently, the last ones (ILs) are the most interesting due to their unique properties such as low toxicity, high polarity, non-flammability, lower vapor pressure, excellent solubility, and thermal stability (Verma et al., 2017). Thus, these salts were investigated as catalysts and biocatalysts in food science (Zhang et al., 2017), antimicrobial activity (Nicosia et al., 2015) as media for the metal electro-deposition (Chu et al., 2014), and recently as ecological inhibitors to minimize the corrosion rate of metals when are in contact with aggressive solutions (El-Hajjaji et al., 2019; Qiang et al., 2017). This interest in ILs comes from the association of inorganic anion ligation such as bromide, iodide, chloride, and organic cations such as *N*-alkyl imidazolium, alkyl phosphonium, alkyl pyridinium or alkyl ammonium (Messali, 2015). This association can result in a phenomenon of intermolecular synergism. The large organic cation of these ILs results in a high inhibition behavior toward the corrosion process in aggressive solution, as many researchers have reported (Verma et al., 2018; El-Hajjaji et al., 2019). El-hajjaji et al., 2019, have investigated the effect of 1-(3-phenoxypropyl) pyridazin-1-ium bromide, as new pyridazinium derivative corrosion inhibitor for mild steel in a 1.0 M HCl solution using electrochemical impedance and XPS spectroscopy. They found

that this derivative has achieved an inhibition of 91% at the optimum concentration of 1.0×10^{-3} M (El-hajjaji et al., 2019). On the other hand, the research was oriented to the application of the imidazolium derivative as cation of ILs. Therefore, El-Katori et al., 2021, have tested the inhibition efficiency of a new chloride imidazolium against the corrosion process of stainless steel using various methods. They reported that these molecules showed a high inhibition performance (around 90%) at low concentration of 120 ppm. They said that the largest size of the molecule displaces significant amount of H_2O molecules from the steel surface and that are adsorbed by hetero-atoms and π -electrons, resulting in the creation of a protective film. Therefore, the inhibition performance enhanced with the increase of the carbon chain alkyl. On another paper, El-Katori et al., 2021, investigated two ionic liquids of imidazolium cation and Brom element as anion. They found that these compounds showed a high inhibition performance against the corrosion process of mild steel immersed in 1.0 M HCl (El-Katori et al., 2021). Furthermore, Ardakani et al., 2020, have investigated the corrosion inhibition performance of new polymeric IL as a green inhibitor for mild steel in 1.0 M HCl solution using various experimental methods. They reported high inhibition efficiency.

The present work focuses on the evaluation of two novel synthesized ionic liquids derived from imidazolium namely: 3-(4-hydroxybutyl)-1-phenethyl-1H-imidazol-3-ium chloride ([HB-Imid] Cl), and 3-(2-chlorobenzyl)-1-phenethyl-1H-imidazol-3-ium chloride ([CB-Imid] Cl) as corrosion inhibitors for mild steel in 1.0 M HCl solution. This study was carried out in order to study the inhibition efficiency between alkyl chain and aromatic ring using electrochemical techniques, characterization surface analysis, and confirmed with a theoretical approach based on DFT calculation and Molecular dynamic simulation.

2. Experimental part

2.1. Chemical synthesis and characterization of ILs inhibitors

The alkyl halides: 4-chlorobutan-1-ol and / or 1-chloro-2-(chloromethyl) benzene (1.1 eq) were added to a solution of 1-phenethyl-1H-imidazole (1 eq) in toluene. The solution was then treated with irradiation for 20 min in a closed vessel at 80 °C using a CEM Microwave. The completion of the reaction was indicated by the formation of an oil from the initially clear homogenous mixture composed of 1-phenethyl-1H-imidazole and the alkyl halide in toluene. The product was extracted with ethyl 2-chloroacetate and ethyl acetate. The IL was then dried at reduced pressure (Fig. 1). The synthesis of these ILs was performed in the Chemistry Department, Faculty of Science, Taibah University, 30002 Al-Madinah Al-Mounawwara, Saudi Arabia.

2.1.1. Characterization of 3-(4-hydroxybutyl)-1-phenethyl-1H-imidazol-3-ium chloride ([HB-Imid] Cl).

FT-IR, cm^{-1} : $\nu = 747$ (Csp³-H, CH₂), 2800 (Csp³-H, CH₂), 1548 (C-H, Csp²-H), 1650 (C = C), 1061 (C-O), 1154 (C-N), 1561 (C = N), and 2874 and 3100 (Ar-H), 3311 (O-H). **¹H NMR** (400 MHz, CDCl₃): δ H = 1.91 (quint, 2H, CH₂), 1.96 (quint, 2H, CH₂), 3.08 (t, 2H, CH₂), 3.36 (t, 2H, CH₂), 4.23 (t, 2H, CH₃), 4.44 (t, 2H, CH₂), 5.17 (s, H, O-H), 7.22–7.57 (d, 2H, Ar-H), 6.62–7.39 (m, 5H, Ar-H), 9.49 (s, 1H,

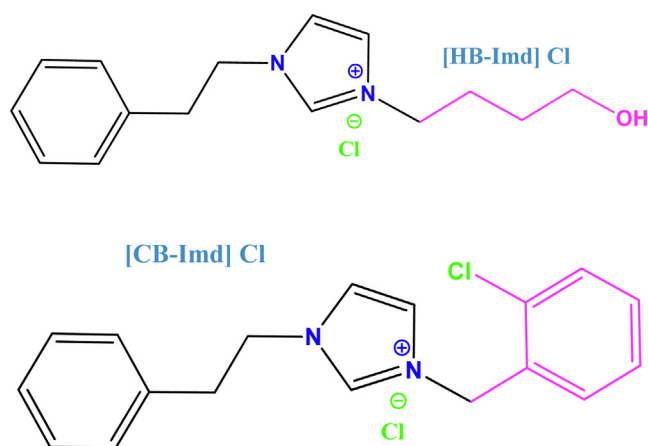


Fig. 1 The studied imidazolium ILs.

Ar-H). **13C NMR** (100 MHz, CDCl₃): δ C = 32.5 (CH₂), 36.2 (CH₂), 46.7 (CH₂), 50.8 (CH₂), 56.9 (CH₂), 59.9 (CH₂), 122.4 (CH), 122.6 (CH), 128.7 (CH), 128.8 (CH), 135.7 (C), and 136.3 (CH). **EA (%)**: Found: C (64.22), H (7.49), N (10.05). Calcd. For C₁₅H₂₁ClN₂O, C (64.16), H (7.54), N(9.98) (**SI. 1**).

2.1.1.1. Characterization of 3-(2-chlorobenzyl)-1-phenethyl-1H-imidazol-3-ium chloride ([CB-Imid] Cl). **FT-IR**, cm⁻¹: ν = 747 (Csp³-H, CH₂), 2805(Csp³-H), 1540 (1154 (C-N), 1548 (C-H, Csp²-H), 1658 (C = C), 1561 (C = N), and 2852 and 3108 (Ar-H). **1H NMR** (400 MHz, CDCl₃): δ H = 3.17 (t, 2H, CH₂), 4.57 (t, 2H, CH₂), 4.55 (s, 2H, CH₂), 7.37–7.61 (d, 2H, Ar-H), 7.01–7.59 (m, 9H, Ar-H), and 10.24 (s, 1H, Ar-H). **13C NMR** (100 MHz, CDCl₃): δ C = 36.34 (CH₂), 50.6 (CH₂), 51.13 (CH₂), 121.6 (CH), 122.6 (CH), 127.3 (CH), 128.1 (CH), 128.9 (CH), 130.0 (CH), 131.1 (CH), 131.7(C), 133.3 (C), 135.7(C), and 137.3 (CH); **EA (%)** Found: C (64.94), H (5.37), N (8.50). Calcd. For C₁₈H₁₈Cl₂N₂, C (64.87), H (5.44), N (8.41) (**SI. 1**).

2.2. Materials and solutions

The mild steel samples used in the present study were composed of Fe (99.30%), S (0.05%), P (0.09%), Si (0.38%), Al (0.01%), Mn (0.05%), and C (0.21%). The surface of these samples was polished with SiC Emery paper with a grain size ranging from 180 to 1500. These samples were degreased with acetone, washed with distilled water, and dried before each test. The molar hydrochloric acid was prepared by dilution of commercial acid (37% HCl: Fischer Scientific) using distilled water. The inhibited solutions concentration ranged from 1.0×10^{-5} M and 1.0×10^{-3} M.

2.3. Electrochemical experiments

The electrochemical experiments were performed using Versa-STAT 4 potentiostat which is controlled with versa-studio analyses software. The electrochemical cell setup consisted of three-electrode system: mild steel with a surface area of 1.0 cm² as the working electrode, platinum as the counter electrode, and Ag/AgCl as the reference electrode. In each experiment, the mild steel sample was stabilized in the aggressive solution for \varnothing h. This investigation was performed in the Engineering Laboratory of Organometallic, Molecular Materials, and Environment, Faculty of Sciences, University Sidi Mohamed Ben Abdellah, Fez, Morocco.

The potentiodynamic polarization curves (PDP) were recorded by varying the electrode potential automatically by ± 250 mV based on the open circuit potential with a scanning rate of 1 mV/s. The inhibition efficiency (η_{PDP} %) was calculated from the corrosion current densities values using **equation (1)** (El Hajjaji et al., 2019).

$$IE_{PDP} = \frac{i_{corr} - i_{corr}^{inh}}{i_{corr}} \times 100 \quad (1)$$

Where IE_{PDP} is the inhibition efficiency, i_{corr} and i_{corr}^{inh} are the current densities without and with the presence of inhibitor, respectively.

In the Nyquist plots, the frequency was set from 100 kHz to 100 mHz and the amplitude was 10 mV using the AC signal at the OCP. These loops were plotted and analyzed using suitable

equivalent circuit. The inhibition efficiency was calculated using **equation (2)** (El Hajjaji et al., 2019).

$$IE_{EIS} = \frac{R_p^{inh} - R_p}{R_p^{inh}} \times 100 \quad (2)$$

Where IE_{EIS} is the inhibition efficiency, R_p^{inh} and R_p represent the polarization resistance in the presence and the absence of inhibitor, respectively.

2.4. Theoretical and computational details

The DFT calculations and molecular dynamic simulation were performed at TUBITAK ULAKBIM, High Performance and Grid Computing Center (TRUBA resources). G09W (Frisch et al., 2013) package was utilized to conduct all the B3LYP (Becke, 1993; Lee et al., 1988) level and 6-311G(df,pd) (McLean and Chandler, 1980; Raghavachari et al., 1980) basis set computations in the gas and water media. ‘‘Polarizable Continuum Model’’ (PCM) (Tomasi et al., 2005; Cossi et al., 2002) was used to perform the water media calculations. GaussView 6.0.16 (GaussView 6.0.16, Gaussian, Inc, Wallingford CT, 2016) was also used to analyze and visualize all computations. All stable structures of [HB-Imid] Cl and [CB-Imid] Cl molecules were verified by the absence of negative frequency.

For the prediction of the chemical reactivity, the HOMO and LUMO energies are of great importance to determine I ‘‘ionization energy’’ and A ‘‘electron affinity’’. In this respect, the Koopmans’ Theorem (Koopmans, 1934) introduced approximately the I and A values via using the FMO energies as follows:

$$I = -E_{HOMO} \quad (3)$$

$$A = -E_{LUMO} \quad (4)$$

Similarly, to the Koopmans theorem, the numerical values of I and A based on the conceptual DFT (Geerlings et al., 2003; Geerlings et al., 2020; Chakraborty and Chattaraj, 2021) have been commonly used to calculate the reactivity parameters and thus the evaluation of the relevant chemical and/or physical process. Thus, the main reactivity parameters, which are χ ‘‘electronic chemical potential’’, η ‘‘global hardness’’, ω ‘‘electrophilicity’’, and ΔN_{max} ‘‘the maximum charge transfer index’’, are given in the following equations (Parr et al., 1999; Parr and Pearson, 1983; Pearson, 1986):

$$\chi = -\frac{I + A}{2} \quad (5)$$

$$\eta = \frac{I - A}{2} \quad (6)$$

$$\omega = \frac{\mu^2}{2\eta} \quad (7)$$

$$\Delta N_{max} = \frac{I + A}{2(I - A)} \quad (8)$$

Besides, ΔN ‘‘fractional number of the electrons transferred’’ is when the B and C systems are together and a contact between them happens, and can be calculated using the following equation (Pearson, 1988):

$$\Delta N = \frac{\chi_C - \chi_B}{2(\eta_C + \eta_B)} \quad (9)$$

Furthermore, the metal-inhibitor interaction energy ($\Delta\psi$) for a corrosion process (Sastri and Perumareddi, 1997) can be calculated by the equation (10):

$$\Delta\psi = -\frac{(\phi_M - \chi_{inh})^2}{4(\eta_M + \eta_{inh})} \quad (10)$$

Recently, ω^- “the electro-donating power” and ω^+ “the electro-accepting power” (Gazquez et al., 2007) are getting used increasingly to calculate the possible electronic tendency of a specific molecular system in the ground state.

$$\omega^+ \approx \frac{(I + 3A)^2}{16(I - A)} \quad (11)$$

$$\omega^- \approx \frac{(3I + A)^2}{16(I - A)} \quad (12)$$

In addition, $\Delta E_{back-donation}$ “back-donation energy” value (Gomez et al., 2006) gives a foresight of the molecular system stability and is calculated using the following equation:

$$\Delta E_{back-donation} = -\frac{\eta}{4} \quad (13)$$

2.5. Molecular Dynamics simulation studies

In order to get further insights under atomic-scale, the molecular dynamic calculations were carried out under solvation conditions using 100 H₂O + 4Cl⁻ + 3 H₃O⁺ solution’s composition. This was performed in a simulation box of 25 Å × 25 Å × 94 Å, which comprises 8 Fe(110) layers with 11 × 11 Fe atoms per face and 80 Å as a vacuum region. The temperature of the studied systems was fixed at 298 K through Andersen’s thermostat. At the time of simulation, 250 ps were selected with 1 fs as a time step. All calculations were conducted under periodic boundary conditions and employing COMPASS as a force field. Ewald and atom-based summation methods were used to compute the electrostatic and the Van der Waals interactions, respectively (Rizvi et al., 2021).

To predict the adsorption and binding energies for the studied chemical systems, the following equations are used (Guo et al., 2017):

$$E_{ads} = E_{total} - (E_{solution+metal} + E_{inhibitor}) \quad (14)$$

$$E_{binding} = -E_{ads} \quad (15)$$

In these equations, E_{total} , and $E_{solution+metal}$ represent the total energy of the system and the total energy of the system without any inhibitor molecule, respectively. $E_{inhibitor}$ represents the energy of the inhibitor molecule.

The type of interactions between the adsorbent and the adsorbate can be expected by using the length of established interfacial bonds. In this regard, the radial distribution function (noted $g(r)$) was analyzed to determine the minimal inter-atomic distance at the inhibitor/metal interface. The last radial function is defined as the probability of finding particle B within the range ($r + dr$) around particle A and is calculated according to equation (16).

$$g_{AB}(r) = \frac{1}{\langle \rho_B \rangle_{local}} \times \frac{1}{N_A} \sum_{i \in A} \sum_{j \in B} \frac{\delta(r_{ij} - r)}{4\pi r^2} \quad (16)$$

Amorphous cell and Forcite tools in Material Studio V.6 was used the estimation of mean square displacement (MSD). Calculations were performed with 30 inhibitors, 3Cl⁻ and 3

H₃O⁺ ions considering COMPASS force field. Van der Waals and electrostatic interactions were determined in the light of group-based method. For the calculation of MSD and diffusion coefficients (D), the following formulae are used:

$$MDS(t) = \langle |r_i(t) - r_i(0)|^2 \rangle \quad (17)$$

$$D = \frac{1}{6N} \lim_{t \rightarrow \infty} \frac{d}{dt} \sum_{i=1}^N \langle |r_i(t) - r_i(0)|^2 \rangle \quad (18)$$

Where $r_i(t)$ and $r_i(0)$ denote the position of atom i in the t moment and in the initial moment, respectively, whereas N is the number of particles in the system.

2.6. Surface analysis

In order to obtain information about the adsorption behavior of these ILs inhibitors, a scanning electron microscope (SEM) (QUATTRO S FEG, thermo-scientific microscopy) was used after an immersion time of 6 h with and without an optimum concentration (1.0×10^{-3} M) of the studied inhibitors. The composition of the material was obtained using an energy dispersive X-ray (EDX) instrument attached to the scanning electron microscopy with an acceleration voltage of 20 kV. This analysis was performed in National Center for Scientific and Technical Research (CNRST).

3. Results and discussions

3.1. Potentiodynamic polarization analysis

3.1.1. Concentration effect of the studied ILs

The polarization curves of mild steel specimens in [HB-Imid] Cl, and [CB-Imid] Cl at 298 K are showed in Fig. 2. The electrochemical parameters were extracted and encapsulated in Table 1.

First, the polarization curves of the studied ILs showed an important decrease in the corrosion current density compared to the uninhibited solution. The decrease in the corrosion current density was greater for [HB-Imid] Cl compound than that for [CB-Imid] Cl. As Fig. 3 showed, the corrosion current density decreased with the increase of inhibitors concentration, signifying the decrease in the corrosion rate process. In addition, by comparing the shapes of the obtained polarization curves, the contribution of these inhibitors could be detected to control hydrogen evolution (Han et al., 2020). This inspection was confirmed by the determinate values of current densities i_{corr} listed in Table 1, and were achieving an inhibition efficiency of 95.9% for [HB-Imid] Cl, and 95.7% for [CB-Imid] Cl at the maximum concentration (1.0×10^{-3} M).

Therefore, it was concluded that the inhibition performance showed a small increase in the presence of the alkyl chain in [HB-Imid] Cl molecule compared to the phenyl chloride group in the [CB-Imid] Cl compound.

On another side, it is well known that the appearance of the second line indicates the presence of the desorption process. In our case, the anodic zone showed a remarkable desorption effect in the potential greater than -250 mV. This potential is defined as the desorption potential explained therefore by desorption of the adsorbed molecules from the mild steel surface (Tana et al., 2019). In addition, the small variation in the

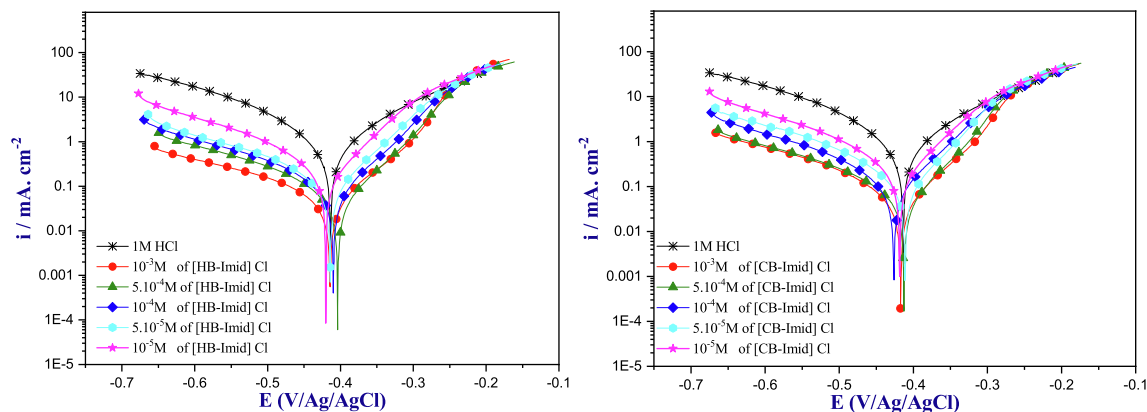


Fig. 2 Potentiodynamic polarization curves of steel surface in 1.0 M HCl solution without and with ILs inhibitors concentrations.

Table 1 Potentiodynamic polarization parameters of mild steel surface in 1.0 M HCl solution without and with ILs inhibitors at different concentrations.

Medium	Conc. (M)	E_{corr} (mV vs. Ag/AgCl)	i_{corr} ($\mu\text{A cm}^{-2}$)	$-\beta_c$ (mV dec ⁻¹)	β_a (mV dec ⁻¹)	η_{pp} %
1 M HCl	**	-413	944	139	128	**
[HB-Imid] Cl	1.0×10^{-5}	-420	245	133	79	74.0
	5.0×10^{-5}	-414	105	130	72	88.8
	1.0×10^{-4}	-409	75	124	68	92.0
	5.0×10^{-4}	-404	54	129	66	94.2
	1.0×10^{-3}	-414	35	123	63	96.2
[CB-Imid] Cl	1.0×10^{-5}	-418	265	132	79	71.9
	5.0×10^{-5}	-410	127	125	667	86.5
	1.0×10^{-4}	-425	106	127	73	88.8
	5.0×10^{-4}	-412	53	129	61	94.3
	1.0×10^{-3}	-416	48	122	64	94.9

cathodic slope values signifies that no modification was shown in the cathodic mechanism.

It is well known that the inhibitors could act as anodic or cathodic types if the displacement of E_{corr} values in inhibited solution is more than 85 mV compared to that of the uninhibited one. While, if the changes of the E_{corr} values is less than 85 mV, they act as mixed-type inhibitor (El-Hajjaji et al., 2020). In the present work, the studied ILs derivatives were classified as mixed-type inhibitors since the E_{corr} values were less than 85 mV. Furthermore, it can be seen that these molecules adsorbed on the mild steel surface samples by blocking both the cathodic and anodic sites.

3.1.2. Temperature effect of studied ILs

It is well known that the inhibition performance can be affected by the rise of temperature effect (Ech-chihbi et al., 2017). Therefore, the temperature effect was evaluated using the polarization Tafel curves technique in order to study the inhibition performance of these ILs. The obtained polarization curves of the mild steel surface in the presence and the absence of the optimum inhibitor concentration (1.0×10^{-3} M) at various temperatures (298 K to 328 K) are presented in Fig. 3, while the various electrochemical parameters are listed in Table 2.

First, it can be seen from the shape of the polarization plots that the current density values increase with the increase of the temperature. This increase is more pronounced in the uninhib-

ited solutions compared to that of the inhibited ones, which indicates an adsorption behavior of these molecules. Table 2 shows that the i_{corr} values increased from $35 \mu\text{A cm}^{-2}$ to $309 \mu\text{A cm}^{-2}$ for [HB-Imid] Cl, and from $48 \mu\text{A cm}^{-2}$ to $436 \mu\text{A cm}^{-2}$ for [CB-Imid] Cl when the temperature was raised from 298 K to 328 K; consequently, the inhibition efficiency decreased slightly with the increase of temperature. This decrease is more for the [CB-Imid] Cl molecule than that for the [HB-Imid] Cl molecule. Based on the inhibition efficiency, the studied ILs compounds showed a small decrease with the increase in temperatures indicating their chemical adsorption (Fouda et al., 2019).

In order to estimate some thermodynamic parameters such as the activation energy (E_a), the activation enthalpy (ΔH^*), and the activation entropy (ΔS^*) for the corrosion of the studied mild steel in 1.0 M HCl in the absence and presence of studied inhibitors, Arrhenius equation, and its alternative formulation were applied to these parameters to provide more information on the corrosion inhibition mechanism (Table 3). The Arrhenius equation (Eq. (19)) and its alternative formulation (transition state) (Eq. (20)) were determined as follows (Saady et al., 2021):

$$i_{corr} = A e^{\left(\frac{-E_a}{RT}\right)} \quad (19)$$

$$i_{corr} = \frac{RT}{Nh} e^{\left(\frac{\Delta S^*}{R}\right)} e^{\left(\frac{-\Delta H^*}{RT}\right)} \quad (20)$$

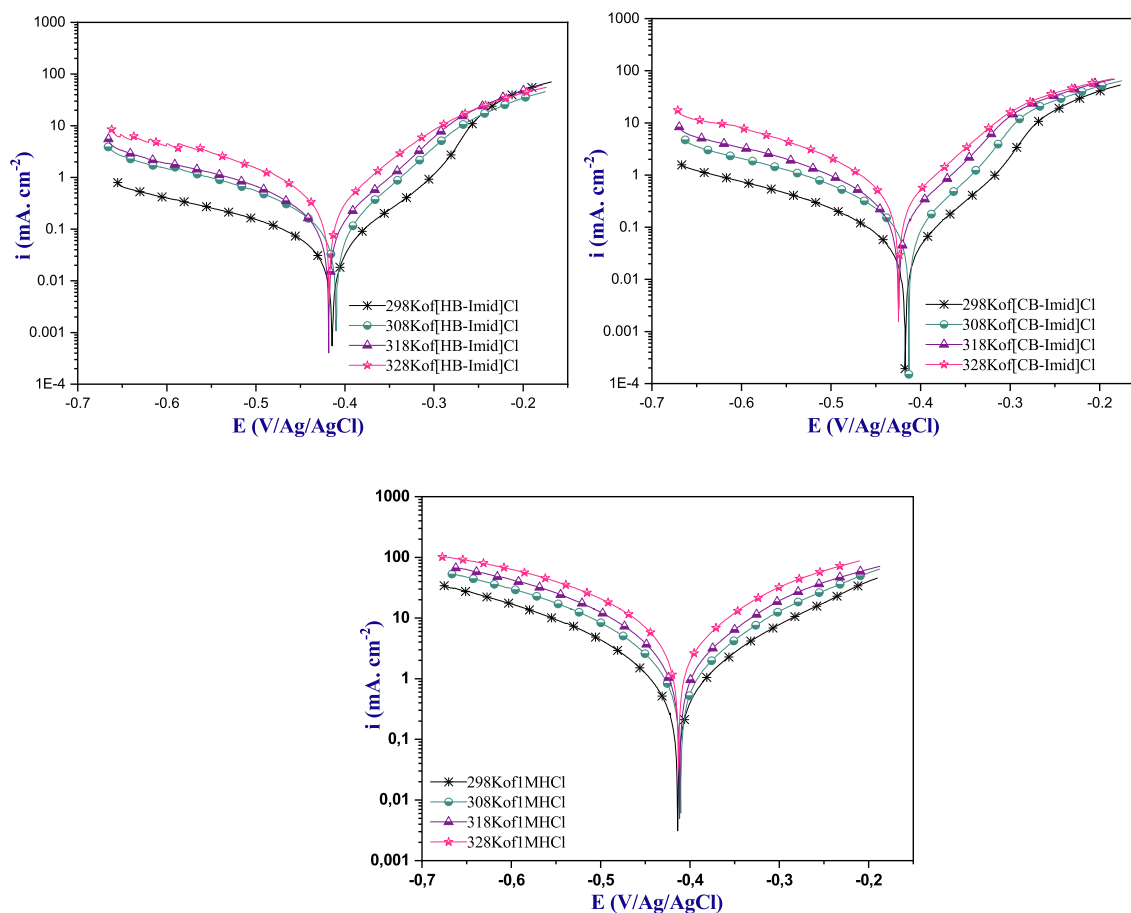


Fig. 3 Polarization curves of mild steel in 1.0 M HCl with and without ILs inhibitors at various temperatures.

Table 2 Electrochemical parameters for mild steel in 1.0 M HCl in the presence and absence of studied 1.0×10^{-3} M ILs at various temperatures (298 K-328 K).

Medium	Temp. (K)	$-E_{corr}$ (mV vs. Ag/AgCl)	i_{corr} ($\mu A cm^{-2}$)	$-\beta_c$ (mV dec $^{-1}$)	β_a (mV dec $^{-1}$)	η_{PP} %
1.0 M HCl	298	413	944	139	128	–
	308	410	1690	137	129	–
	318	411	2328	126	125	–
	328	412	3387	120	133	–
1.0 $\times 10^{-3}$ M [HB-Imid] Cl	298	414	35	123	63	96.2
	308	410	94	110	68	94.4
	318	418	162	129	75	93.0
	328	418	309	110	81	90.8
1.0 $\times 10^{-3}$ M [CB-Imid] Cl	298	416	48	122	64	94.9
	308	412	135	126	63	92.0
	318	424	232	122	71	90.0
	328	424	436	110	79	87.1

Where T is the absolute temperature, N is the Avogadro's number, h is the Plank's constant, and R is the gas constant. The activation energy, E_a , for the mild steel in uninhibited and inhibited solution was deduced from the linear square fits of $\ln i_{corr}$ versus $(1000/T)$ while ΔH^* and ΔS^* were obtained from the linear square fits of $\ln(i_{corr}/T)$ versus $(1000/T)$ (Fig. 4). The regression coefficient (R^2) of these plots was

found to be 0.998 confirming the confidentiality of the kinetic activation parameters obtained.

From Table 3, it is clear that the E_a in the presence of the studied salts are greater than that in the uninhibited solution. This increase in the activation energy signifies the formation of electrostatic bonds between the mild steel surface (Fe) and the studied ILs molecules (Faydy et al., 2019).

Table 3 Thermodynamic adsorption parameters in 1.0 M HCl without and with optimum concentration.

Thermodynamic parameters	1.0 M HCl	[HB-Imid] Cl	[CB-Imid] Cl
E_a (KJ mol ⁻¹)	33.86	57.7	58.4
ΔH^* (KJ mol ⁻¹)	31.26	55.1	55.8
ΔS^* (J mol ⁻¹ K ⁻¹)	-82.73	-29.8	-24.7

The activation enthalpy values with both inhibitors are superior with a positive sign than that of the blank solution, reflecting the endothermic process of the studied ILs, and indicating a delayed dissolution reaction of the studied steel.

Furthermore, the less negative values of the activation entropy for the studied compounds indicate the formation of a structured stable layer on the steel specimen's surface when compared with the uninhibited solution (Zhang et al., 2012). From these results, it can be concluded that the adsorption process of these salts was very complex.

3.2. Electrochemical impedance spectroscopy of the studied ILs

3.2.1. Concentration effect of the studied ILs

The inhibition behavior of the studied ILs was also evaluated using EIS technique. The Nyquist and bode presentation for mild steel with and without adding various ILs concentrations are presented in Fig. 5, while their Electrochemical parameters were regrouped in Table 4 after a good simulation as the EIS plots have showed.

First, it is clear from Fig. 5 that the shapes of the Nyquist curves did not show perfect semicircles which is probably due to the steel surface heterogeneity caused by the existence of impurities, roughness, inhibitor adsorption, etc. (Ech-chihbi et al., 2020). Therefore, in order to get a great simulation of these curves, the constant phase element (CPE (n , Q)) was performed instead of the pure capacitor because it takes into consideration the depression of the obtained plots (Fig. 6). Moreover, these plots were having only one semicircle indicating that the mechanism of corrosion reactions was controlled by charge transfer (Ech-chihbi et al., 2020).

The charge transfer mechanism was also confirmed by Bode's presentation since detecting only one single-phase peak in the mid-frequency range. In addition, a single time constant was identified for the two ILs molecules taking place at the metal/electrolyte interface. These phase angles were smaller than -90° , indicating the depression obtained in the shape of Nyquist plots, and confirming the equivalent mentioned circuit (Dehghani et al., 2020). Furthermore, the phase angle increased with the increase of the studied ILs concentration, which is directly correlated to the adsorption of imidazolium-based ILs onto the mild steel surface and thus the formation of a protective layer (Dehghani et al., 2020).

The effective capacity (C_{dl}) was determined by the following mathematical formula (Eq. (21)) where Q is the constant phase angle (CPE), R_p is the polarization resistance, and n is the heterogeneity values of surface ($0 < n < 1$) (El Faydy et al., 2018).

$$C_{dl} = \left(Q \times R_p^{1-n} \right)^{1/n} \quad (21)$$

It is clear from Table 4 that the R_p values (polarization resistance) enhanced with the increase of the studied ILs concentrations reaching a maximum value of $815.4 \Omega \text{ cm}^2$ for [HB-Imid] Cl, and $770 \Omega \text{ cm}^2$ for [CB-Imid] Cl at the optimum concentration of $1.0 \times 10^{-3} \text{ M}$. Whereas, the element phase constant (Q) and the capacitive double layer C_{dl} decreased slightly. As Table 4 showed, the C_{dl} increased from 13.0 to $36.7 \mu\text{F cm}^{-2}$ with [CB-Imid] Cl, and from 11.9 to $30.7 \mu\text{F cm}^{-2}$ with [HB-Imid] Cl. This result indicates that the studied inhibitors acted as smart molecules that can be adsorbed onto the metal surface creating a barrier film blocking the contact mild steel / hydrochloric acid solution (Arrouse et al., 2020). This behavior was also confirmed by the calculated inhibition efficiencies which reached 95.9%, and 95.7% for [HB-Imid] Cl, and [CB-Imid] Cl at the optimum concentration ($1.0 \times 10^{-3} \text{ M}$), respectively. By comparing these two molecules, the difference can be due to the presence of the alkyl chain which covered a large surface area of the mild steel surface. On the other hand, [CB-Imid] Cl molecule structure has phenyl group which perhaps deviated the adsorption despite the C = C bonds. This difference makes a small difference in the inhibition performance. Finally, it can be concluded that the EIS analysis goes

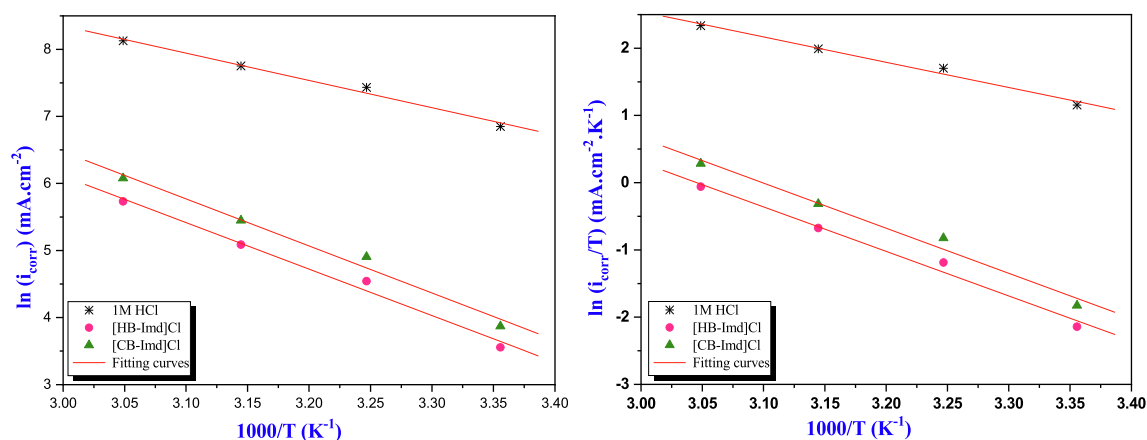


Fig. 4 Arrhenius and transition state plots for mild steel in 1.0 M HCl solution without and with optimum concentration of the studied ILs.

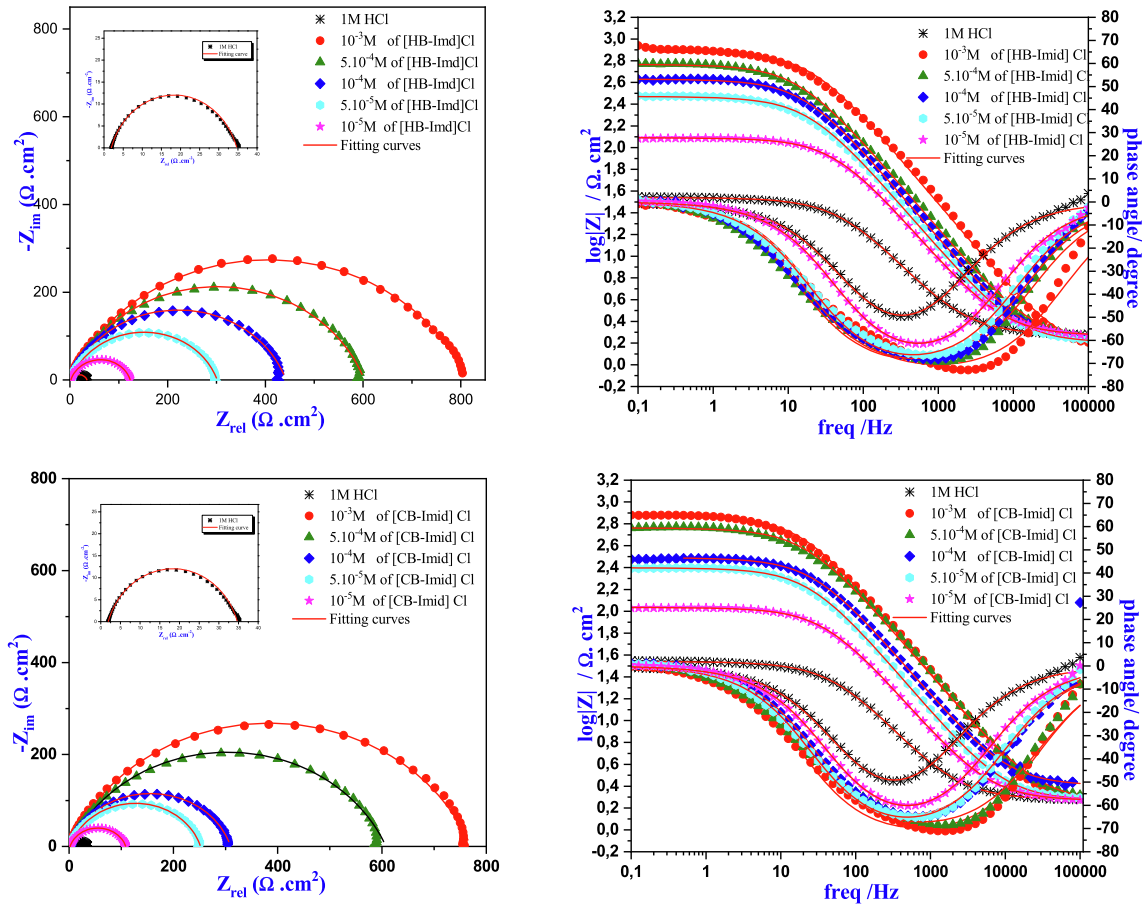


Fig. 5 Nyquist plots and bode diagrams for studied ILs in 1.0 M HCl at various concentrations.

Table 4 Impedance parameters for the mild steel in 1.0 M HCl solution without and with different concentration of studied ILs at 298 K.

Medium	Conc. (M)	$R_s(\Omega \text{ cm}^2)$	$R_p(\Omega \text{ cm}^2)$	CPE		$C_{dl}(\mu\text{F cm}^{-2})$	θ	$\eta_{imp}\%$
				$Q (\mu\text{F S}^{n_{dl}})$	n_{dl}			
Cl	1.0	1.7	33	312.7	0.784	89.1	—	—
[HB-Imid] Cl	1.0×10^{-5}	1.8	121.4	81.6	0.825	30.7	0.728	72.8
	5.0×10^{-5}	1.5	299.7	76.3	0.799	29.6	0.889	88.9
	1.0×10^{-4}	1.5	440.4	60.9	0.798	24.4	0.925	92.5
	5.0×10^{-4}	1.6	601.0	54.8	0.785	21.6	0.945	94.5
	1.0×10^{-3}	1.2	815.4	37.4	0.753	11.9	0.959	95.9
[CB-Imid] Cl	1.0×10^{-5}	1.8	106.7	99.2	0.820	36.7	0.690	69.0
	5.0×10^{-5}	1.9	249.8	68.4	0.820	26.6	0.867	86.7
	1.0×10^{-4}	0.8	307.3	46.2	0.818	18.0	0.892	89.2
	5.0×10^{-4}	0.5	607.1	44.7	0.757	14.1	0.945	94.5
	1.0×10^{-3}	0.2	770.0	36.6	0.775	13.0	0.957	95.7



Fig. 6 Equivalent circuit used in experimental impedance fit.

with the same trend as those obtained by the potentiodynamic polarization technique which led us to suggest that these ILs act as good inhibitors against corrosion of mild steel in 1.0 M HCl solution.

3.2.2. Adsorption isotherms of the studied ILs

The Adsorption isotherms models are appropriate and important in order to get information about the adsorption mecha-

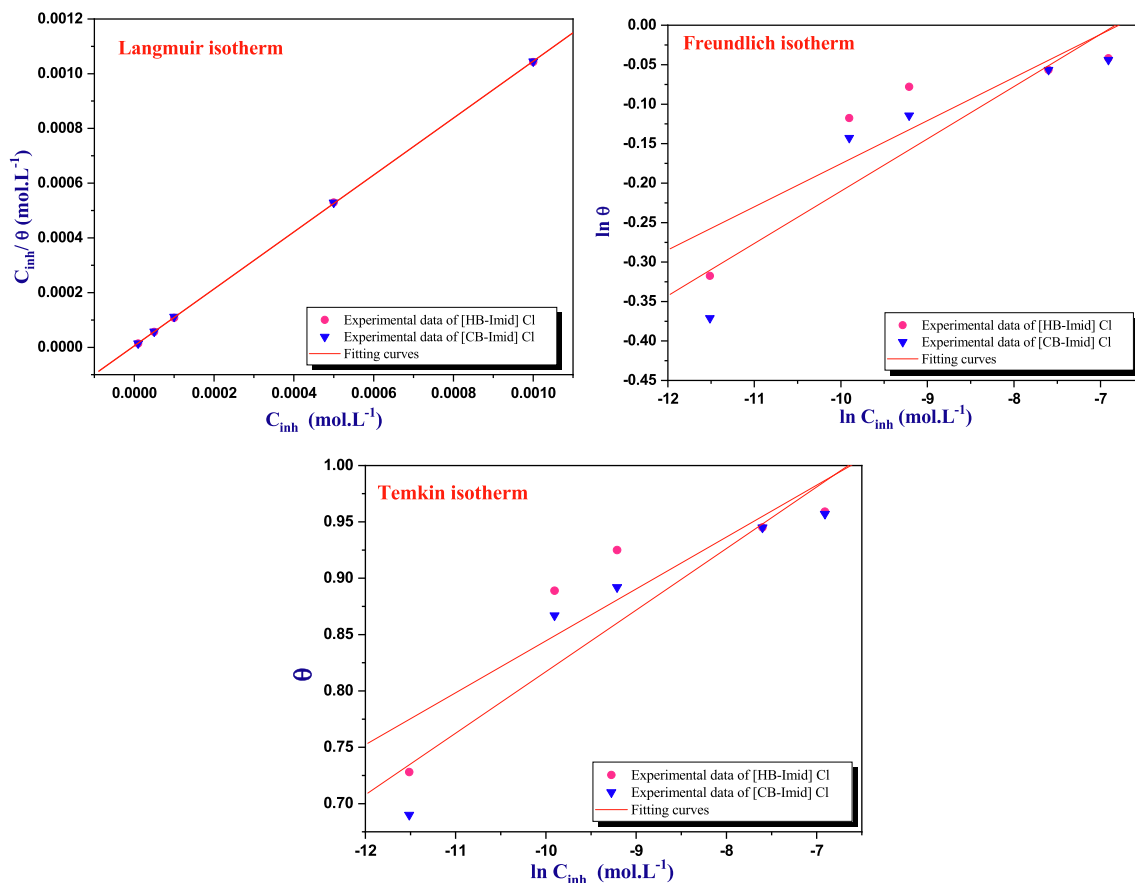


Fig. 7 Adsorption isotherms models for studied ILs at 298 K.

Table 5 Isotherm models parameters for the studied ILs.

Isotherms	Inhibitors	R^2	Parameters	K	ΔG_{ads}° (KJ mol $^{-1}$)	
Langmuir	[HB-Imid] Cl	0.999	slope	1.040	2.15×10^5	-40.4
	[CB-Imid] Cl	0.999		1.040	1.57×10^5	-39.6
Freundlich	[HB-Imid] Cl	0.889	n	18.32	1.45	-10.8
	[CB-Imid] Cl	0.919		15.09	1.57	-11.0
Temkin	[HB-Imid] Cl	0.901	a	-10.80	2.03×10^{12}	-80.2
	[CB-Imid] Cl	0.934		-9.15	6.95×10^{10}	-71.8

nism of the inhibitors onto the metal surface (Salim et al., 2017). Thus, the adsorption isotherms models of [HB-Imid] Cl, and [CB-Imid] Cl ionic liquids on the MS surface were performed to study the interaction between the mild steel samples and these Imidazolium-based inhibitors using Langmuir, Temkin, and Freundlich isotherms and based on the results obtained from EIS (Fig. 7). The adsorption parameters for these ILs in 1.0 M HCl obtained from Langmuir, Freundlich, and Temkin isotherms are summarized in Table 5.

The linear equations of these isotherms are:

$$\text{Langmuir isotherm} \frac{C_{inh}}{\theta} = \frac{1}{K_{ads/des}} + C_{inh} \frac{C_{inh}}{\theta} \text{ vs } C_{inh} \quad (22)$$

$$\text{Temkin isotherm} : \theta = \frac{-1}{2a} \ln(K_{ads/des}) - \frac{1}{2a} \ln(C_{inh}) \theta \text{ vs } \ln(C_{inh}) \quad (23)$$

$$\ln \theta = \ln K_{ads/des} + \frac{1}{n} \ln C_{inh} \ln(\theta) \text{ vs } \ln(C_{inh}) \quad (24)$$

where θ is the degree of surface coverage, C_{inh} is the inhibitor concentration, $K_{ads/des}$ is the equilibrium constant of the adsorption/desorption process, and a is the molecular lateral interactions ($a > 0$; attraction), ($a < 0$; repulsion).

Moreover, the expression of standard Gibb's free energy of adsorption was applied to calculate ΔG_{ads}° using the following equation (25) (Chauhan et al., 2019).

$$\Delta G_{ads}^{\circ} = -RT \ln(55.5 K_{ads/des}) \quad (25)$$

With 55.5 is the molar concentration of H₂O in solution, R is the universal gas constant (8.314 J mol $^{-1}$ K $^{-1}$), and T is the absolute temperature.

From the studied isotherms models, it is clear that [HB-Imid] Cl, and [CB-Imid] Cl ionic liquids obey the Langmuir

isotherm because both parameters, the regression coefficient and the slope (a), are the closest to the unity (1.04 for both compounds) (Ituen et al., 2017). For the Freundlich isotherm, both compounds do not obey this isotherm since the adsorption constant, K_{ads} , has no signification (very small values). On the other side, the Temkin isotherm model showed a high value of K_{ads} and regression coefficient compared to the Freundlich model which leads us to say that these compounds can also obey this model. In addition, [HB-Imid] Cl, and [CB-Imid] Cl may be having a repulsive interaction since having a negative value of the parameters (a) (Verma et al., 2019).

In the literature, the physical adsorption nature was detected between charged metal and charged inhibitor if ΔG_{ads} value is around -20 kJ mol^{-1} or less in negative value, while chemisorptions nature was present if the ΔG_{ads} value is around -40 kJ mol^{-1} or more in negative value (Nahlé et al., 2021). In our case, the ΔG_{ads} values as shown in Table 5 are $-40.4 \text{ KJ mol}^{-1}$, and $-39.6 \text{ KJ mol}^{-1}$ for [HB-Imid] Cl, and [CB-Imid] Cl, respectively. As a result, the obtained findings reveal that the adsorption of the examined ILs is mainly chemisorption i.e. adsorbed onto the steel surface and forming strong bonds.

3.2.3. Immersed time of studied ILs

The behavior of the investigated ILs [HB-Imid] Cl, and [CB-Imid] Cl was studied with the increase of time scale using EIS technique. This study was performed for the blank (1.0 M HCl) and inhibited solution (containing

$1.0 \times 10^{-3} \text{ M}$) at various immersion times ranging from 0 h to 12 h. The recorded impedance diagrams are shown in Fig. 8 while the electrochemical parameters were listed in Table 6.

It can be seen from Fig. 8 that the Nyquist diagram for [HB-Imid] Cl, and [CB-Imid] Cl showed a loop of one single depressed semicircle which decreased with the increase of immersion time. In addition, this small decrease indicates that these ionic liquids acted as good inhibitors even during the very long immersion time.

The results obtained from the immersion time revealed that the R_p value diminished slightly with the enhancement of the immersion time from $770.0 \Omega \text{ cm}^2$ to $114.4 \Omega \text{ cm}^2$ for [CB-Imid] Cl; and from $815.4 \Omega \text{ cm}^2$ to $127.0 \Omega \text{ cm}^2$ for [HB-Imid] Cl. At the same time, the double layer capacitance (C_{dl}) increased slowly with the increase of immersion time.

Moreover, it can be seen from the calculated inhibition efficiencies that both inhibitors showed a small decrease until the time of 4 h, and then stayed almost stable until 12 h. Finally, it can be concluded that the two molecules showed a high inhibition behavior with the immersion time confirming that they can be adsorbed on the mild steel surface creating a protective layer (Singh et al., 2018).

3.3. Surface analysis (MEB-EDX)

The surface analysis of the immersed specimens in the uninhibited and inhibited solution for 6 h at 298 K was performed to

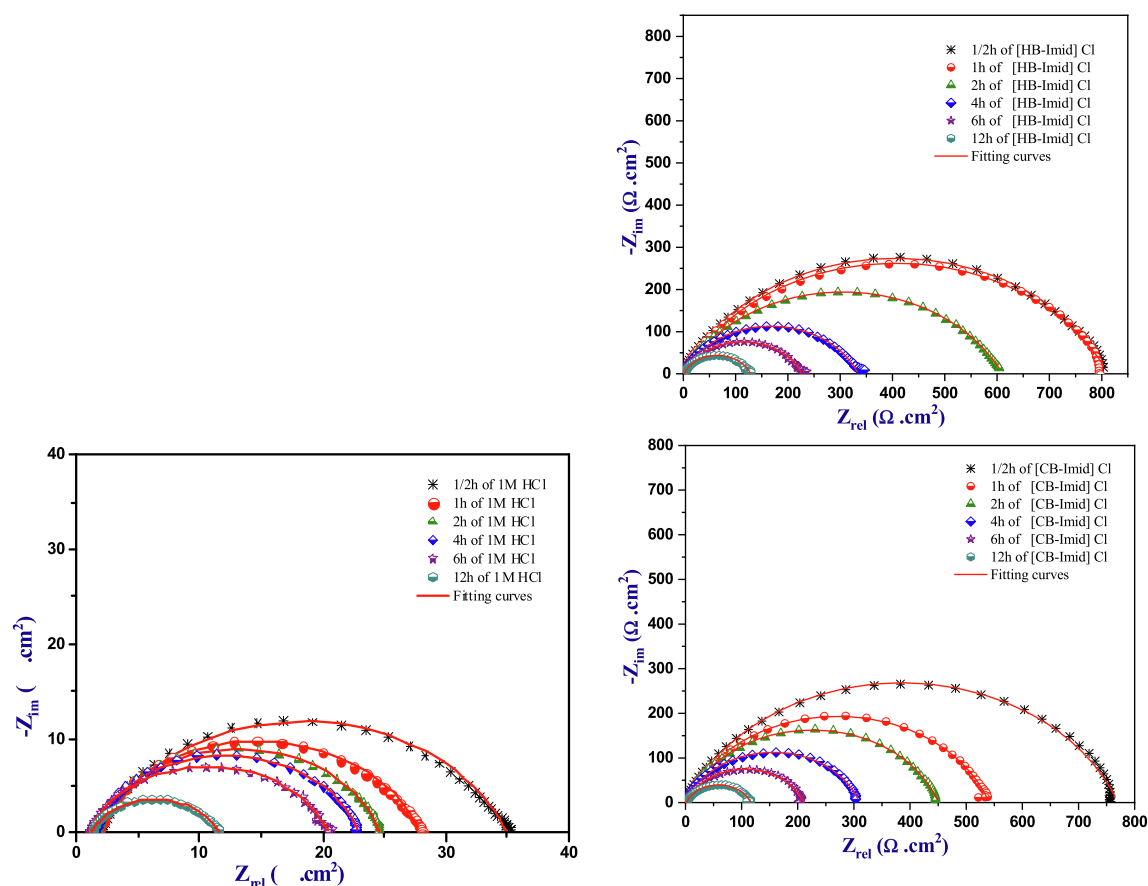


Fig. 8 Nyquist plots for mild steel in 1.0 M HCl with and without the studied inhibitors at different immersion time.

Table 6 Electrochemical parameters in 1.0 M HCl without and with different immersion time of the studied ILs.

Medium	Time (h)	R_s ($\Omega\text{ cm}^2$)	R_p ($\Omega\text{ cm}^2$)	Q ($\mu\text{F S}^{-1}$)	n_{dl}	C_{dl} ($\mu\text{F cm}^{-2}$)	η_{imp} %
1.0 M HCl	1/2	1.7	33.0	312.70	0.784	89.1	**
	1	1.6	26.4	364.90	0.810	122.7	**
	2	1.5	23.0	433.0	0.835	174.3	**
	4	1.5	21.4	627.00	0.834	267.0	**
	6	1.0	19.4	963.80	0.796	349.4	**
	12	1.2	10.4	949.2	0.764	419.5	**
[HB-Imid] Cl	1/2	1.2	815.4	37.4	0.753	11.9	95.9
	1	0.08	812.6	44.0	0.730	12.8	96.7
	2	0.4	610.7	61.5	0.720	17.2	96.2
	4	0.3	334.2	69.1	0.756	20.5	93.5
	6	0.7	225.9	93.3	0.754	26.4	91.4
	12	1.4	127.0	177.5	0.770	57.1	91.8
[CB-Imid] Cl	1/2	0.2	770.0	36.6	0.775	13.0	95.7
	1	0.9	539.9	54.1	0.791	21.3	95.1
	2	0.8	449.6	54.3	0.797	21.1	94.8
	4	0.8	309.2	63.6	0.800	23.9	93.0
	6	1.2	209.5	93.6	0.789	32.8	90.7
	12	1.6	114.4	218.8	0.771	73.2	90.9

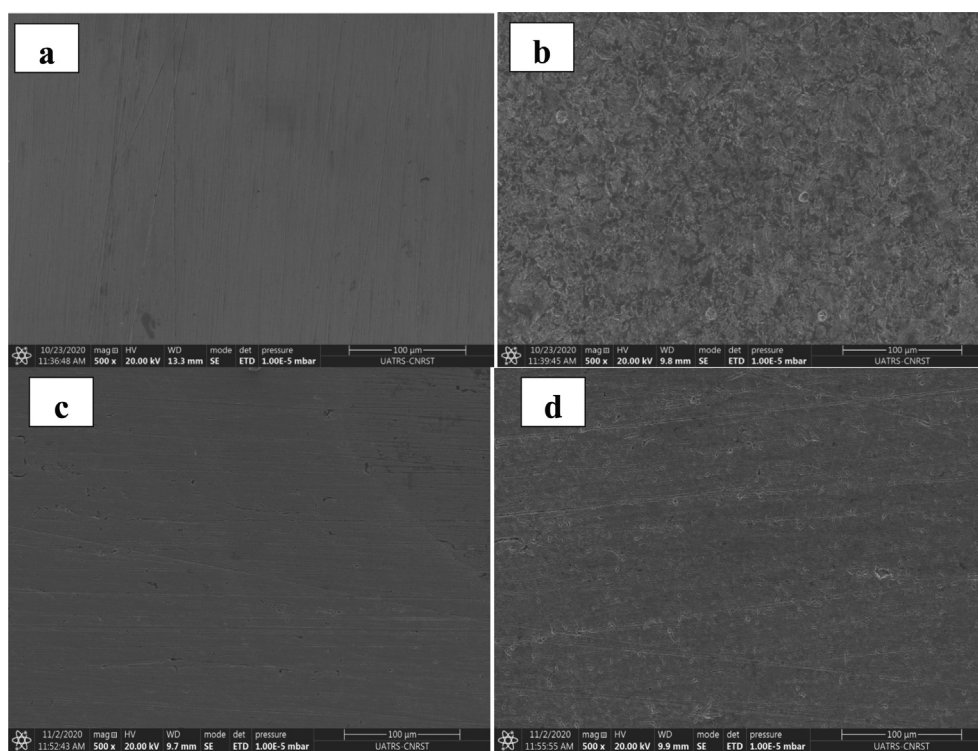


Fig. 9 Micrograph images of mild steel before immersion (a), after immersion in 1.0 M HCl solution (b), after immersion in 1.0 M HCl solution containing 1.0×10^{-3} M [HB-Imid] Cl inhibitor (c), and after immersion in 1.0 M HCl solution containing 1.0×10^{-3} M [CB-Imid] Cl inhibitor (d).

show the morphology and nature of atoms adsorbed on the mild steel surface. First, it can be observed from Fig. 9 (a, b) that the sample after immersion in the acidic medium showed a remarked damages of the steel surface compared to the sur-

face morphology before the immersion time. On the other hand, the samples obtained after their immersion in the inhibited solution was smoother compared to the morphology of sample immersed in acidic media which may be due to the for-

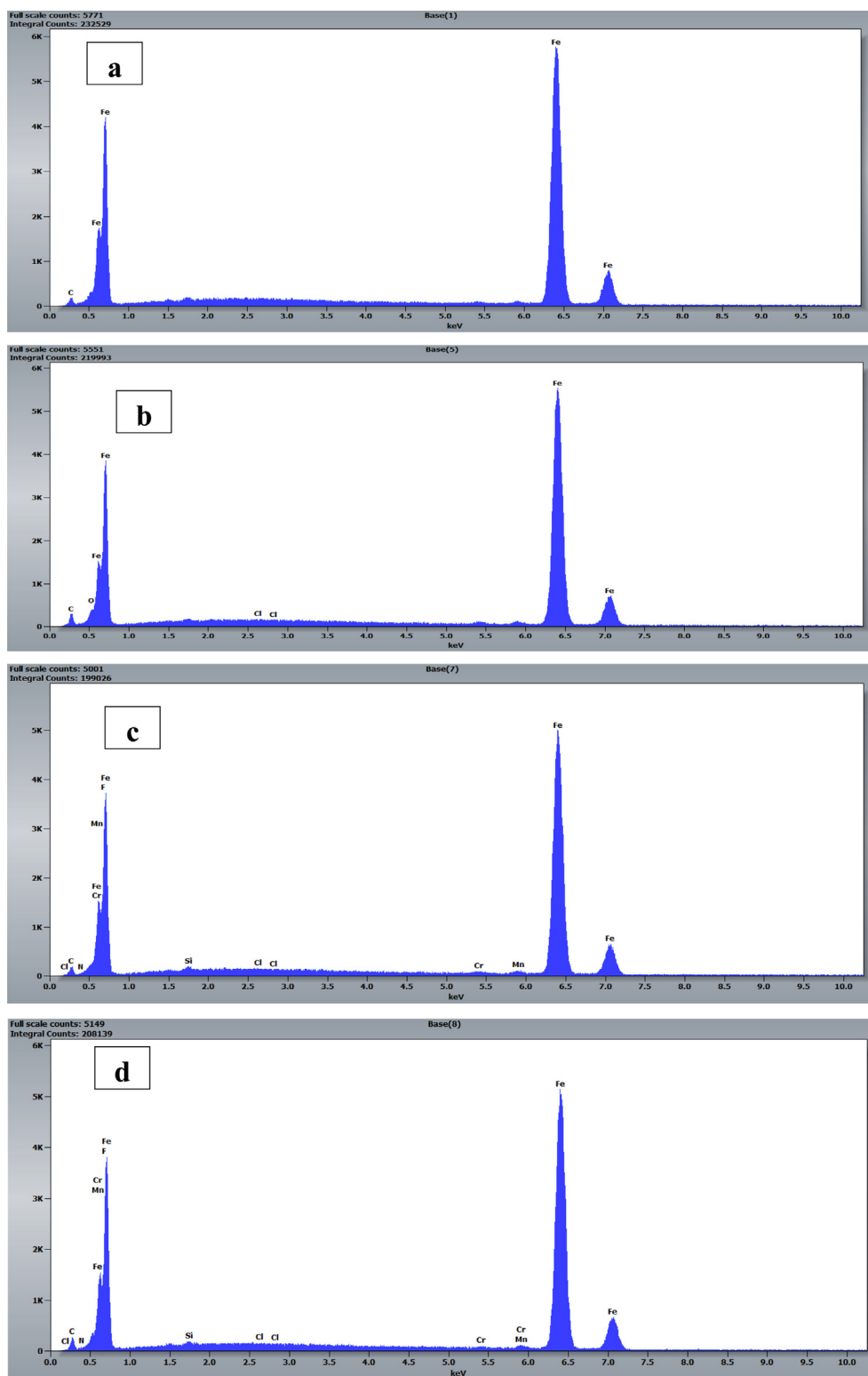


Fig. 10 EDX spectra of mild steel before immersion (a), after immersion in 1.0 M HCl solution (b), after immersion in 1.0 M HCl solution containing 1.0×10^{-3} M of [HB-Imid] Cl inhibitor (c), and after immersion in 1.0 M HCl solution containing 1.0×10^{-3} M of [CB-Imid] Cl inhibitor (d).

mation of heterogeneous protecting layer that formed by the adsorption of the studied ILs forming therefore, a coordination bonds with the steel surface (Fig. 9 (c, d)).

The EDX technique based on the analysis of X-rays emitted during electron-matter interaction was also performed in order to understand the active sites responsible for the adsorption of

Table 7 Weight percentage of the elements obtained from EDX analysis.

specimens	Fe	C	O	Cl	N	Mn	Cr	Si	F
Mild steel	98.50	1.50							
Mild steel + 1.0 M HCl	96.82	2.45	0.65	0.07	–				
Mild steel + [HB-Imid] Cl	94.31	1.85	–	0.06	0.32	1.04	0.27	0.40	1.75
Mild steel + [CB-Imid] Cl	91.68	2.51	–	0.00	0.93	0.99	0.28	0.30	3.32

the studied ILs. EDX allows characterizing the chemical element adsorbed on the steel surface after being immersed in the corrosive medium with and without ILs inhibitors. The spectra obtained before and after the immersion in the absence and the presence of inhibitors are shown in Fig. 10 while the weight percentage of various elements adsorbed on the steel surface are listed in Table 7.

It is observed from Table 7 that various elements were detected using EDX analysis. Also, a small percentage in nitrogen and carbon atoms was showed which lead us to suggest that these atoms may be responsible to make interaction with the mild steel surface. Moreover, it can be seen that the chloride percentage in the presence of [CB-Imid] Cl molecule do not appear which may be due to largest size of the molecule that displaces a significant Cl atom from the surface. On the other hand, the percentage of the iron atom obtained from the inhibited solutions is less than that obtained from the

aggressive solution (1.0 M HCl). Thus, it can be conclude from the EDX microanalysis that the studied ILs adsorb onto the samples surface by nitrogen atom and the C = C bonds making a protective film layer and confirming the good behavior of these molecules when it is in contact with the aggressive solution (1.0 M HCl) (Arrouse et al., 2020).

3.4. Theoretical study

3.4.1. DFT study

The computational tools are widely used to explain or predict the nature of physical and/or chemical phenomena in many fields, especially in engineering and pharmaceutical research (Arrouse et al., 2020). For this purpose, the analysis of FMO energies and densities is very useful and used to investigate the possible reactivity of both simple (Serdaroglu et al., 2020); and complex molecules (Serdaroglu, 2020; Jacob

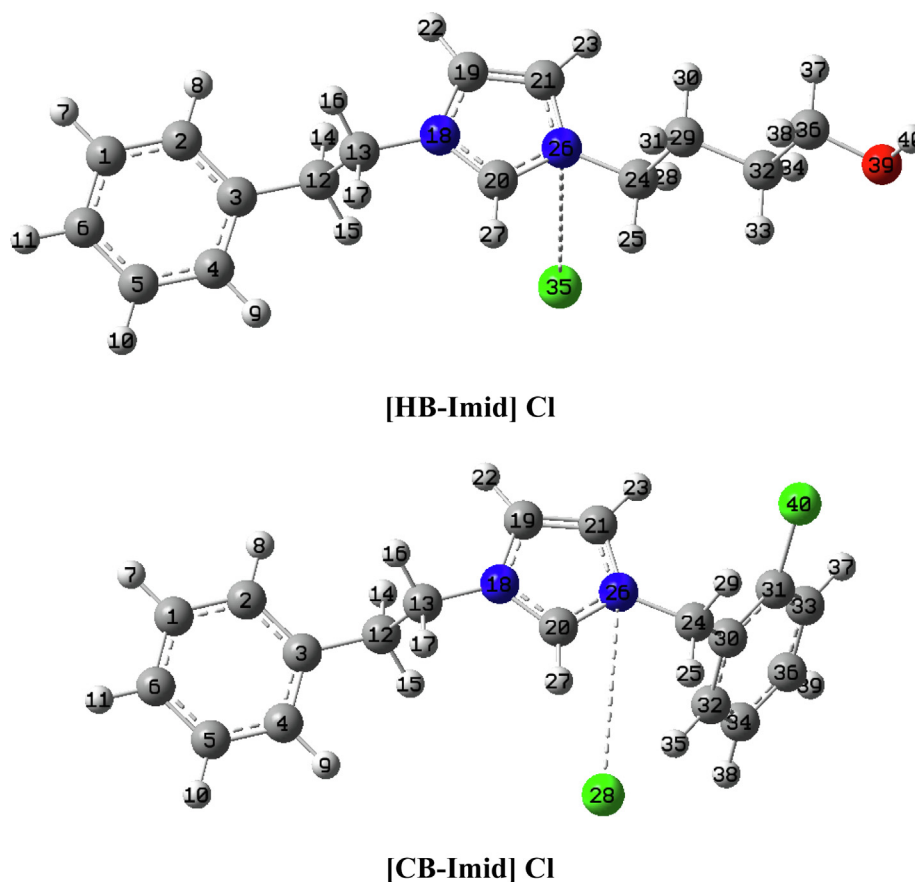
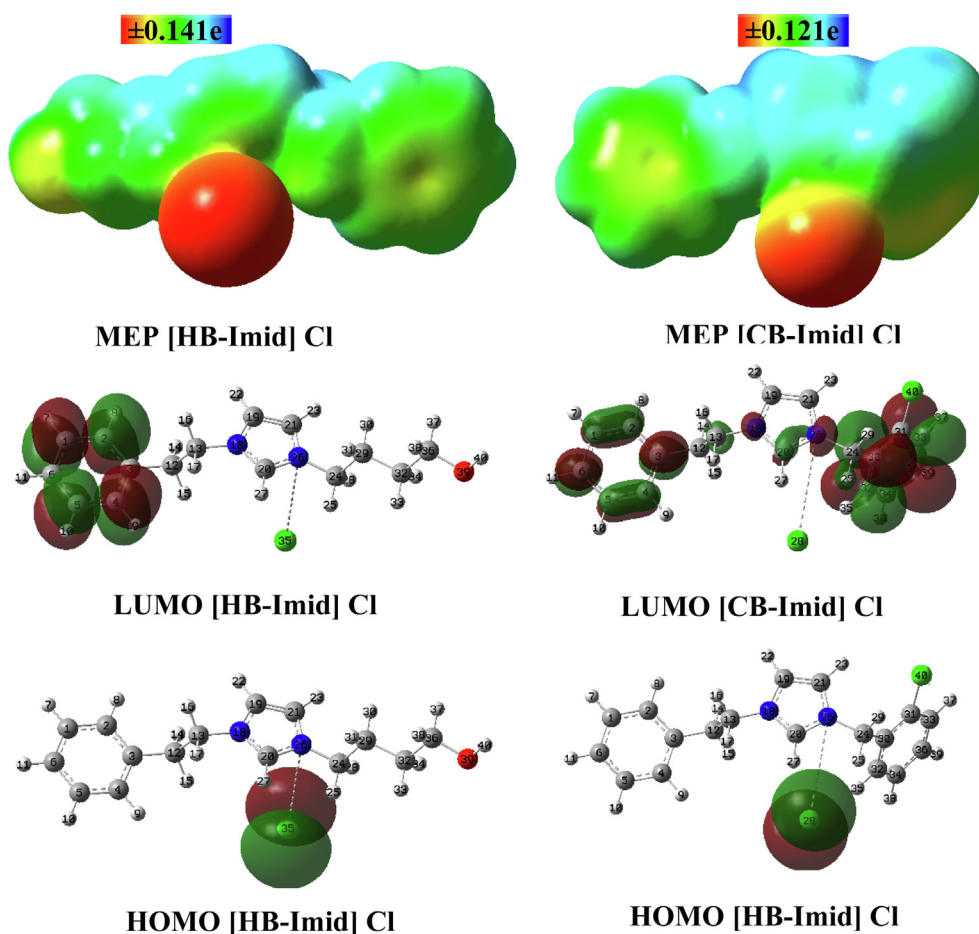


Fig. 11 The optimized structures of the [HB-Imid] Cl and [CB-Imid] Cl compounds at B3LYP/6-311G(df,pd) level in the water phase.

Table 8 Quantum Chemical Parameters of [HB-Imid] Cl and [CB-Imid] Cl compounds at B3LYP/6-311G(df,pd) level.

	Gas		Water	
	[HB-Imid] Cl	[CB-Imid] Cl	[HB-Imid] Cl	[CB-Imid] Cl
HOMO (-I)	-5.3879	-6.7109	-5.5345	-6.8646
LUMO (-A)	-1.1208	-1.0814	-1.3995	-1.2177
ΔE (L-H)	4.2670	5.6295	4.1350	5.6469
μ	-3.2543	-3.8961	-3.4670	-4.0412
η	2.1335	2.8147	2.0675	2.8235
ω	2.4820	2.6965	2.9069	2.8920
ΔN_{max}	1.5253	1.3842	1.6769	1.4313
ω^+	1.1215	1.1003	1.4318	1.2244
ω^-	4.3759	4.9964	4.8988	5.2655
ΔN	0.3669	0.1641	0.3272	0.1379
$\Delta\Psi$	-0.2872	-0.0758	-0.2214	-0.0537
D (debye)	10.5735	23.5092	9.7069	17.6244
α (au)	198.6663	235.8257	232.5633	295.4600

**Fig. 12** HOMO & LUMO (iso value: 0.02) and MEP (iso value: 0.0004) plots of [HB-Imid] Cl and [CB-Imid] Cl compounds at B3LYP/6-311G(df,pd) level.

et al., 2020). In this context, the optimized structures of the inhibitors [HB-Imid] Cl, and [CB-Imid] Cl in the water phase are presented in Fig. 11. Also, the reactivity values calculated by using the FMO energies were given in Table 8. The reactive

sites obtained from both the FMO densities and MEP plots are given in Fig. 12.

Although both the HOMO and LUMO energies of [HB-Imid] Cl, and [CB-Imid] Cl were reduced in the water dielec-

Table 9 Adsorption and binding energies (kcal mol^{-1}) of investigated inhibitor molecules on the iron surface under solvation circumstance.

Molecules	E_{ads}	$E_{Binding}$
[HB-Imid] Cl	-174.027	174.027
[CB-Imid] Cl	-162.826	162.826

tric, the energy gap of the [HB-Imid] Cl molecule narrowed in the water phase and vice versa for [CB-Imid] Cl. Here, it is quite reasonable to say that the [HB-Imid] Cl molecule was

more eager for the intramolecular interactions than the intermolecular interactions in comparison to the [CB-Imid] Cl molecule, in both media. As expected from the aromatic structure of [CB-Imid] Cl, μ values also indicated that the [CB-Imid] Cl was more electronically stable than the [HB-Imid] Cl molecule. By comparing the results of the gas phase, [HB-Imid] Cl molecule was softer in the aqueous environment while [CB-Imid] Cl became harder. Still, it should be noticed that the [HB-Imid] Cl molecule was softer than [CB-Imid] Cl molecule [HB-Imid] Cl (2.1335 eV) < [CB-Imid] Cl (2.8147 eV) in the gas and as [HB-Imid] Cl (2.0675 eV) < [CB-Imid] Cl (2.8235 eV) in the water. Furthermore, [CB-Imid] Cl (2.8147 eV) had more electrophilic character than [HB-Imid]

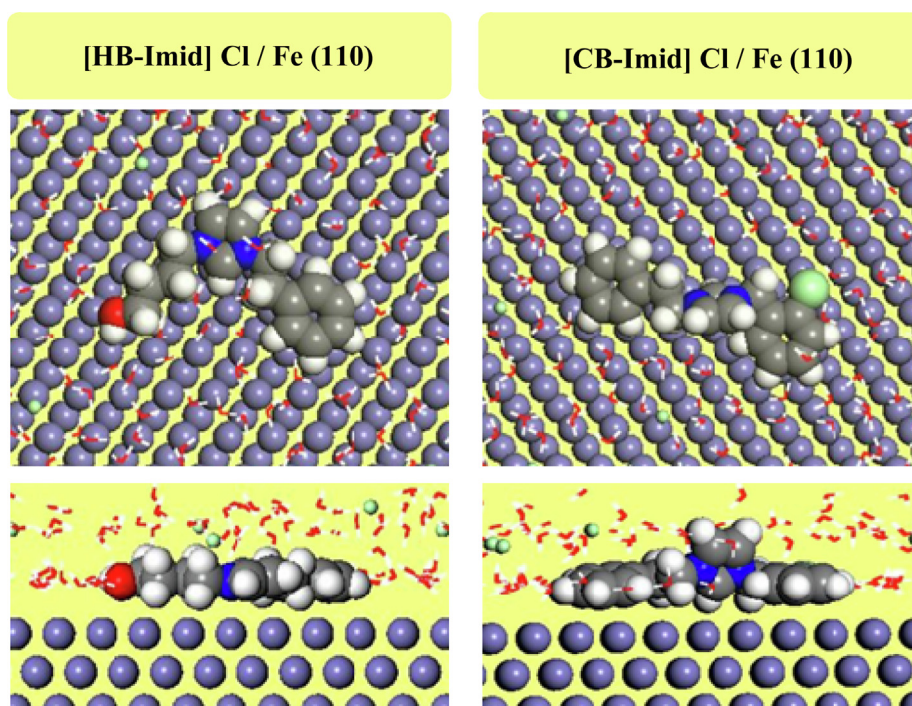


Fig. 13 Top and side-views of the equilibrium adsorption geometry of the examined inhibitors onto the Fe(110) surface after the MD process.

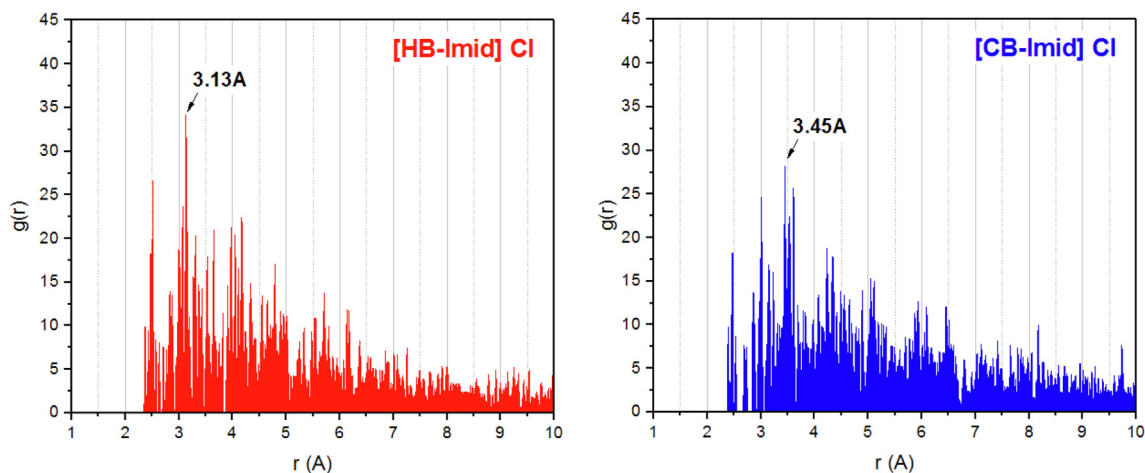


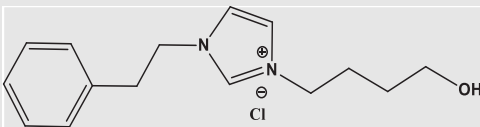
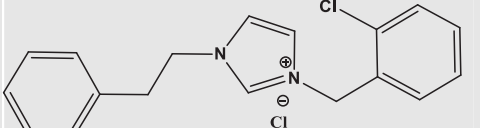
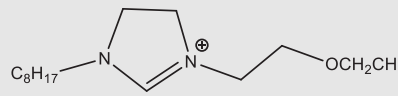
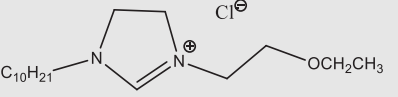
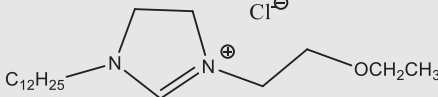
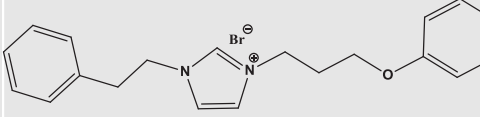
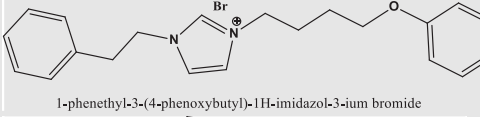
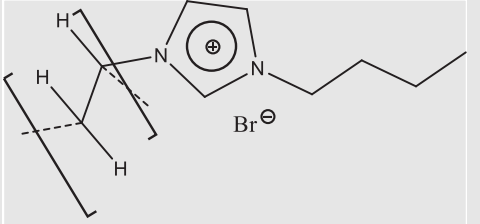
Fig. 14 Radial distribution function (RDF) of the two inhibitors on the Fe(110) surface.

Table 10 Self-diffusion coefficient (D) of Cl^- and H_3O^+ ions through the inhibitors membrane.

Inhibitor	$D \times 10^{-5}$ (cm ² /s)	
	Cl^-	H_3O^+
[HB-Imid] Cl	11.4	11.3
[CB-Imid] Cl	276.7	238.3

Cl (2.1335 eV) in the gas and calculated vice versa in the water. The charge transfer capabilities of both compounds were calculated and found higher in the water than those in the gas phase. In addition, ω^- powers of both compounds were calculated and found greater than ω^+ power, in both phases. It should be announced that the [CB-Imid] Cl had more ω^- power than the [HB-Imid] Cl, in both phases. The ΔN and $\Delta \Psi$ parameters disclosed that the [HB-Imid] Cl molecule would present a good interaction with the metal surface than the [CB-Imid] Cl.

Table 11 Inhibition efficiency percentage of different ILs immersed in acidic medium (HCl).

Molecules	High inhibition percentage	Optimum concentration	Steel / medium	References
 3-(4-hydroxybutyl)-1-phenethyl-1H-imidazol-3-ium chloride	95.9	10^{-3} M	Mild steel in 1.0 M HCl	This work
 3-(2-chlorobenzyl)-1-phenethyl-1H-imidazol-3-ium chloride	95.7	10^{-3} M	stainless steel (201 SS) in 2.0 M HCl	This work
 3-(2-Ethoxymethyl)-1-octyl-1H-imidazol-3-ium chloride	88.1	120 ppm	stainless steel (201 SS) in 2.0 M HCl	(El-Katori et al., 2021)
 1-Decyl-3-(2-ethoxymethyl)-1H-imidazol-3-ium chloride	90.4	120 ppm	stainless steel (201 SS) in 2.0 M HCl	(El-Katori et al., 2021)
 1-Dodecyl-3-(2-ethoxymethyl)-1H-imidazol-3-ium chloride	91.5	120 ppm	stainless steel (201 SS) in 2.0 M HCl	(El-Katori et al., 2021)
 1-phenethyl-3-(3-phenoxypropyl)-1H-imidazol-3-ium bromide	85.8	10^{-3} M	Mild steel in 1.0 M HCl	(ElHajjaji et al., 2021)
 1-phenethyl-3-(4-phenoxybutyl)-1H-imidazol-3-ium bromide	96.7	10^{-3} M	Mild steel in 1.0 M HCl	(ElHajjaji et al., 2021)
 poly [3-butyl-1-vinylimidazolium bromide]	92.0		Mild steel in 1.0 M HCl	(Ardakani et al., 2020)

Namely, the ΔN values changed as [HB-Imid] Cl (0.3669 eV) > [CB-Imid] Cl (0.1641 eV) in the gas and as [HB-Imid] Cl (0.3272 eV) > [CB-Imid] Cl (0.1379 eV) in the water. In addition, $\Delta\psi$ values were calculated as [HB-Imid] Cl (-0.2872 eV) < [CB-Imid] Cl (-0.0758 eV) in the gas and as [HB-Imid] Cl (-0.2214 eV) < [CB-Imid] Cl (-0.0537 eV) in the water, which was a proof that [HB-Imid] Cl could interact more strongly with the metal surface than [CB-Imid] Cl.

From Fig. 12, the HOMO density as a sign of the nucleophilic attack site for [HB-Imid] Cl and [CB-Imid] Cl expanded over the chlorine, whereas the LUMO density as a marker of the electrophilic attack site was spread out on the Phenyl- rings, for both compounds. For both compounds, the chlorine atom would have a significant role in electrophilic attacks because it was covered quite in the red color ($V < 0$) that demonstrated the electron-rich region. In addition, the H atom closer to the -N-Cl fragment of both compounds seems blue ($V > 0$) color that was a mark as the electron-poor region for the nucleophilic attacks. In addition, the Phenyl- ring(s) for both compounds were covered by yellow color as an indicator of the lower size negative electrostatic potential. The electrostatic potential for [HB-Imid] Cl changed in the range ± 0.141 e, whereas it was calculated in the range ± 0.121 e for [CB-Imid] Cl, which showed that the charge distribution on [HB-Imid] Cl changed over a wider range compared to those for [CB-Imid] Cl.

3.4.2. Molecular dynamic calculations

Molecular Dynamics Simulation Approach (Guo et al., 2017) can be considered as a powerful tool in terms of highlighting the adsorption characteristics of inhibitor molecules. The calculated adsorption and binding energies are important indicators of corrosion inhibition efficiencies of molecules (Erdoğan et al., 2017). It should be noted that more negative adsorption energies are obtained for more effective corrosion inhibitors. Table 9 shows the calculated adsorption and binding energies for [HB-Imid] Cl + Fe (110) and [CB-Imid] Cl + Fe (110) systems. In Fig. 13, the most stable adsorption modes for the studied molecules are presented. It is apparent from the data presented in the related Table that [HB-Imid] Cl molecule is a more effective corrosion inhibitor than [CB-Imid] Cl. This result is in good agreement with the experiments made.

To accomplish the geometric inspection of the adsorption geometry of studied organic inhibitors, the radial distribution function (RDF) was analyzed. RDF is a suitable computational tool to estimate the inter-atomic distance between two species (adsorbed inhibitor and surface). Distances between 1.0 and 3.5 Å generally correspond to chemical bond, while non-bonding one, i.e. physical interaction, is associated with distances longer than 3.5 Å. Fig. 14 shows the pair correlation functions of the two inhibitors onto the Fe(110) surface. As can be seen, the maximum value of the $g(r)$ function corresponds to 3.13 and 3.45 Å for [HB-Imid] Cl and [CB-Imid] Cl inhibitors, respectively. This indicates the possibility of studied inhibitors to adsorb strongly (i.e., chemisorption) onto the metal surface, which is more important in the case of [HB-Imid] Cl as it shows lower inter-atomic distance. This proposes the strong interaction of [HB-Imid] Cl inhibitor on Fe(110) surface compared to [CB-Imid] Cl one, which consists with obtained E_{ads} values and explains further the achieved inhibition efficiencies.

Another way for evaluating the corrosion inhibition performances of the studied inhibitors is to calculate and use the self-diffusion coefficient (noted as D) of corrosive species, namely Cl^- and H_3O^+ ions via inhibitor membranes (Table 10). The diffusion ability of corrosive species can be predicted from the calculated D values. From tabulated values, it is apparent that [HB-Imid] Cl (lower D values) prevents favorably the diffusion of selected corrosive agents via inhibitor membrane than the [CB-Imid] Cl inhibitor. This leads to the protection of MS surface against the corrosion, which supports our experimental findings.

Finally, it can be concluded that the ILs show a good inhibition performance with a deviation percentage that due to the different alkyl cationic form used and the alkyl group used. Table 11 reports the percentage inhibition efficiency for some selected ILs with the imidazolium derivatives used as corrosion inhibitors in acidic medium. From the inhibition percentage, it can be concluding that these molecules showed a good inhibition performance for mild steel when they are in contact with the molar hydrochloric acid.

4. Conclusion

The studied ILs acted as good inhibitors against the corrosion of mild steel in 1.0 M HCl media. This conclusion was confirmed by several electrochemical techniques, theoretical approaches, and characterization analysis. It can be concluded that both inhibitors showed high reactivity with a small difference due to the change of the alkyl chain with the benzyl chloride. Moreover, the PDP technique confirms the inhibition efficiencies reached with the EIS method, and that these molecules are classified as a mixed type inhibitors. Furthermore, the studied ILs inhibitors obey Langmuir isotherm models by forming protective layer on the steel surface which is also confirmed by MEB-EDX surface analysis. The DFT/B3LYP/6-311G(df,pd) results revealed that the [CB-Imid] Cl molecule was more polarizable, soft, and had a lower electron-donating capability than the [HB-Imid] Cl. Besides, FMO analysis implied that the chlorine atom on the parent molecules would be important in the nucleophilic attacks for both molecules.

Declaration of Competing Interest

The authors declare that they have no known competing financial interests or personal relationships that could have appeared to influence the work reported in this paper.

Acknowledgments

The DFT calculations were performed by Dr. Goncagül Serdaroglu, at TUBITAK ULAKBIM, High Performance and Grid Computing Center (TRUBA resources).

Appendix A. Supplementary data

Supplementary data to this article can be found online at <https://doi.org/10.1016/j.arabjc.2022.103967>.

References

- Ardakani, E.K., Kowsari, E., Ehsani, A., 2020. Imidazolium-derived polymeric ionic liquid as a green inhibitor for corrosion inhibition of mild steel in 1.0 M HCl: Experimental and computational study. *Colloids Surf. A Physicochem. Eng. Asp.* 586, 1241957.

- Arrousse, N., Salim, R., Kaddouri, Y., Zahri, D., El Hajjaji, F., Touzani, R., Taleb, M., Jodeh, S., 2020. The inhibition behavior of Two pyrimidine-pyrazole derivatives against corrosion in hydrochloric solution: Experimental, surface analysis and in silico approach studies. *Arabian J. Chem.* 13, 5949–5965.
- Becke, A.D., 1993. A new mixing of Hartree-Fock and local density-functional theories. *J. Chem. Phys.* 98, 1372–1377.
- Bouoidina, A., Ech-chihbi, E., El-Hajjaji, F., El Ibrahim, B., Kaya, S., Taleb, M., 2020. Anisole derivatives as sustainable-green inhibitors for mild steel corrosion in 1 M HCl: DFT and molecular dynamic simulations approach. *J. Mol. Liq.* 324, 115088.
- Chakraborty, D., Chattaraj, P.K., 2021. Conceptual density functional theory based electronic structure principles. *Chem. Sci.* 12, 6264–6279.
- Chauhan, D.S., Quraishi, M.A., Sorour, A.A., Saha, S.K., Banerjee, P., 2019. Triazole-modified chitosan: a biomacromolecule as a new environmentally benign corrosion inhibitor for carbon steel in a hydrochloric acid solution. *RSC Adv.* 9 (26), 14990–15003.
- Chu, Q., Liang, J., Hao, J., 2014. Electrodeposition of zinc-cobalt alloys from choline chloride–urea ionic liquid. *Electrochim. Acta* 115, 499–503.
- Cossi, M., Scalmani, G., Rega, N., Barone, V., 2002. New developments in the polarizable continuum model for quantum mechanical and classical calculations on molecules in solution. *J. Chem. Phys.* 117, 43–54.
- Dehghani, A., Bahlakeh, G., Ramezanzadeh, B., Ramezanzadeh, M., 2020. Potential role of a novel green eco-friendly inhibitor in corrosion inhibition of mild steel in HCl solution: Detailed macro/micro-scale experimental and computational explorations. *Constr. Build. Mater.* 245, 118464.
- Ech-chihbi, E., Belghiti, M.E., Salim, R., Oudda, H., Taleb, M., Benchat, N., Hammouti, B., El-Hajjaji, F., 2017. Experimental and computational studies on the inhibition performance of the organic compound “2-phenylimidazo [1,2-a]pyrimidine-3-carbaldehyde” against the corrosion of carbon steel in 1.0 M HCl solution. *Surf. Interfaces* 9, 206–217.
- Ech-chihbi, E., Nahlé, A., Salim, R., Benhiba, F., Moussaif, A., El-Hajjaji, F., Oudda, H., Guenbour, A., Taleb, M., Warad, I., Zarrouk, A., 2020. Computational, MD simulation, SEM/EDX and experimental studies for understanding adsorption of benzimidazole derivatives as corrosion inhibitors in 1.0 M HCl solution. *Journal of Alloys and Compound* 20, 155842.
- El Faydy, M., Galai, M., Rbaa, M., Ouakki, M., Lakhrissi, B., Ebn Touhami, M., Y., 2018. El Kacimi, Synthesis and Application of New Quinoline as Hydrochloric Acid Corrosion Inhibitor of Carbon Steel. *Anal. Bioanal. Electrochem.* 10 (7), 815–839.
- El Hajjaji, F., Salim, R., Messali, M., Hammouti, B., Chauhan, D., Almutairi, S., Quraishi, M., 2019. Electrochemical Studies on New Pyridinium Derivatives as Corrosion Inhibitors of Carbon Steel in Acidic Medium. *Journal of Bio-and Tribo-Corrosion* 5, 4.
- El-Hajjaji, F., Messali, M., Martínez de Yuso, M.V., Rodríguez-Castellón, E., Almutairi, S., Bandoz, T.J., Algarra, M., 2019. Effect of 1-(3-phenoxypropyl) pyridazin-1-ium bromide on steel corrosion inhibition in acidic medium. *J. Colloid Interface Sci.* 541, 418–424.
- El-Hajjaji, F., Merimi, I., Messali, M., Obaid, R.J., Salim, R., Taleb, M., Hammouti, B., 2019. Experimental and quantum studies of newly synthesized pyridinium derivatives on mild steel in hydrochloric acid medium. *Mater. Today: Proc.* 13, 822–831.
- El-Hajjaji, F., Ech-chihbi, E., Rezki, N., Benhiba, F., Taleb, M., Chauhan, D.S., Quraishi, M.A., 2020. Electrochemical and theoretical insights on the adsorption and corrosion inhibition of novel pyridinium-derived ionic liquids for mild steel in 1 M HCl. *J. Mol. Liq.* 314, 113737.
- ElHajjaji, F., Salim, R., Ech-chihbi, E., Titi, A., Messali, M., Kaya, S., El Ibrahim, B., Taleb, M., 2021. New imidazolium ionic liquids as ecofriendly corrosion inhibitors for mild steel in hydrochloric acid (1 M): Experimental and theoretical approach. *J. Taiwan Inst. Chem. Eng.* 123, 346–362.
- El-Katori, E.E., Nessim, M.I., Deyab, M.A., Shalabi, K., 2021. Electrochemical, XPS and theoretical examination on the corrosion inhibition efficacy of stainless steel via novel imidazolium ionic liquids in acidic solution. *J. Mol. Liq.* 337, 116467.
- Erdoğan, Ş., Safi, Z.S., Kaya, S., Işın, D.Ö., Guo, L., Kaya, C., 2017. A computational study on corrosion inhibition performances of novel quinoline derivatives against the corrosion of iron. *J. Mol. Struct.* 1134, 751–761.
- Faydy, M.E., Rbaa, M., Lakhrissi, L., Lakhrissi, B., Warad, I., Zarrouk, A., Obot, I.B., 2019. Corrosion protection of carbon steel by two newly synthesized benzimidazol-2-ones substituted 8-hydroxyquinoline derivatives in 1 M HCl: Experimental and theoretical study. *Surf. Interfaces* 14, 222–237.
- Fouda, A.S., Ismail, M.A., Al-Khamri, A.A., Abousalem, A.S., 2019. Experimental, quantum chemical and molecular simulation studies on the action of arylthiophene derivatives as acid corrosion inhibitors. *J. Mol. Liq.* 290, 111178.
- Frisch, M.J., Trucks, G.W., Schlegel, H.B., Scuseria, G.E., Robb, M. A., Cheeseman, J.R., Scalmani, G., Barone, V., Mennucci, B., Petersson, G.A., Nakatsuji, H., Caricato, M., Li, X., Hratchian, H. P., Izmaylov, A.F., Bloino, J., Zheng, G., Sonnenberg, J.L., Hada, M., Ehara, M., Toyota, K., Fukuda, R., Hasegawa, J., Ishida, M., Nakajima, T., Honda, Y., Kitao, O., Nakai, H., Vreven, T., Montgomery Jr., J.A., Peralta, J.E., Ogliaro, F., Bearpark, M., Heyd, J.J., Brothers, E., Kudin, K.N., Staroverov, V.N., Keith, T., Kobayashi, R., Normand, J., Raghavachari, K., Rendell, A., Burant, J.C., Iyengar, S.S., Tomasi, J., Cossi, M., Rega, N., Millam, J.M., Klene, M., Knox, J.E., Cross, J.B., Bakken, V., Adamo, C., Jaramillo, J., Gomperts, R., Stratmann, R.E., Yazyev, O., Austin, A.J., Cammi, R., Pomelli, C., Ochterski, J.W., Martin, R.L., Morokuma, K., Zakrzewski, V.G., Voth, G.A., Salvador, P., Dannenberg, J.J., Dapprich, S., Daniels, A.D., Farkas, O., Foresman, J.B., Ortiz, J.V., Cioslowski, J., Fox, D.J., 2013. *Gaussian 09W*, Revision D.01. Gaussian, Inc, Wallingford CT.
- GaussView 6.0.16, Gaussian, Inc, Wallingford CT, 2016.
- Gazquez, J.L., Cedillo, A., Vela, A., 2007. Electrodonating and electroaccepting powers. *J. Phys. Chem. A* 111 (10), 1966–1970.
- Geerlings, P., De Proft, F., Langenaeker, W., 2003. Conceptual Density Functional Theory. *Chem. Rev.* 103 (5), 1793–1874.
- Geerlings, P., Chamorro, E., Chattaraj, P.K., De Proft, F., Gázquez, J. L., Liu, S., Morell, C., Toro-Labbé, A., Vela, A., Ayers, P., 2020. Conceptual density functional theory: status, prospects, issues. *Theor. Chem. Acc.* 139, 36.
- Gomez, B., Likhanova, N.V., Domínguez-Aguilar, M.A., Martínez-Palou, R., Vela, A., Gazquez, J.L., 2006. Quantum Chemical Study of the Inhibitive Properties of 2-Pyridyl-Azoles. *J. Phys. Chem. B* 110 (18), 8928–8934.
- Guo, L., Kaya, S., Obot, I.B., Zheng, X., Qiang, Y., 2017. Toward understanding the anticorrosive mechanism of some thiourea derivatives for carbon steel corrosion: A combined DFT and molecular dynamics investigation. *J. Colloid Interface Sci.* 506, 478–485.
- Guo, Y., Xu, B., Liu, Y., Yang, W., Yin, X., Chen, Y., Le, J., Chen, Z., 2017. Corrosion inhibition properties of two imidazolium ionic liquids with hydrophilic tetrafluoroborate and hydrophobic hexafluorophosphate anions in acid medium. *J. Ind. Eng. Chem.* 56, 234–247.
- Han, T., Guo, J., Zhao, Q., Wu, Y., Zhang, Y., 2020. Enhanced corrosion inhibition of carbon steel by pyridyl gemini surfactants with different alkyl chains. *Mater. Chem. Phys.* 240, 122156.
- Iuen, E., Akaranta, O., James, A., 2017. Evaluation of Performance of Corrosion Inhibitors Using Adsorption Isotherm Models: An Overview. *Chemical Science International Journal* 18, 1–3.
- Jacob, J.M., Kurup, M.R.P., Nisha, K., Serdaroglu, G., Kaya, S., 2020. Mixed ligand copper(II) chelates derived from an O, N, S-

- donortridentate thiosemicarbazone: Synthesis, spectral aspects, FMO, and NBO analysis. *Polyhedron* 189, 114736.
- Koopmans, T., 1934. Über die Zuordnung von Wellenfunktionen und Eigenwerten zu den Einzelnen. *Elektronen Eines Atoms. Physica* 1, 104–113.
- Lee, C., Yang, W., Parr, R.G., 1988. Development of the Colle-Salvetti correlation-energy formula into a functional of the electron density. *Phys. Rev. B* 37, 785–789.
- Marsoul, A., Ijjaali, M., Elhajjaji, F., Taleb, M., Salim, R., Boukir, A., 2020. Phytochemical screening, total phenolic and flavonoid methanolic extract of pomegranate bark (*Punica granatum* L): Evaluation of the inhibitory effect in acidic medium 1 M HCl. *Mater. Today: Proc.* 27, 3193–3198.
- McLean, A.D., Chandler, G.S., 1980. Contracted Gaussian-basis sets for molecular calculations. 1. 2nd row atoms, $Z=11-18$. *J. Chem. Phys.* 72, 5639–5648.
- Messali, M., 2015. Eco-Friendly Synthesis of a New Class of Pyridinium-Based Ionic Liquids with Attractive Antimicrobial Activity. *Molecules* 20, 14936–14949.
- Mohagheghi, A., Arefinia, R., 2018. Corrosion inhibition of carbon steel by dipotassium hydrogen phosphate in alkaline solutions with low chloride contamination. *Constr. Build. Mater.* 187, 760–772.
- Mrani, S.A., El Arrouji, S., Karrouchi, K., El Hajjaji, F., Alaoui, K.I., Rais, Z., Taleb, M., 2018. Inhibitory performance of some Pyrazole derivatives against corrosion of mild steel in 1.0 M HCl: Electrochemical, MEB and theoretical studies. *Int. J. Corros. Scale Inhib.* 7 (4), 542–569.
- Nahlé, A., Salim, R., El Hajjaji, F., Aouad, M.R., Messali, M., Ech-chihbi, E., Hammouti, B., Taleb, M., 2021. Novel triazole derivatives as ecological corrosion inhibitors for mild steel in 1.0 M HCl: experimental & theoretical approach, *RSC. Advances* 11 (7), 4147–4162.
- Nicosia, A., Gieparda, W., Foksowicz-Flaczyk, J., Walentowska, J., Wesolek, D., Vazquez, B., Prodi, F., Belosi, F., 2015. Air filtration and antimicrobial capabilities of electrospun PLA/PHB containing ionic liquid. *Sep. Purif. Technol.* 154, 154–160.
- Nkuna, A.A., Akpan, E.D., Obot, I.B., Verma, C., Ebenso, E.E., Murulana, L.C., 2020. Impact of selected ionic liquids on corrosion protection of mild steel in acidic medium: Experimental and computational studies. *J. Mol. Liq.* 314, 113609.
- Parr, R.G., Pearson, R.G., 1983. Absolute hardness: companion parameter to absolute electronegativity. *J. Am. Chem. Soc.* 105, 7512–7516.
- Parr, R.G., Szentpaly, L.V., Liu, S., 1999. Electrophilicity Index. *J. Am. Chem. Soc.* 121, 1922–1924.
- Pearson, R.G., 1986. Absolute electronegativity and hardness correlated with molecular orbital theory. *Proc. Natl. Acad. Sci. USA* 83, 8440–8441.
- Pearson, R.G., 1988. Absolute Electronegativity and Hardness: Application to Inorganic Chemistry. *Inorg. Chem.* 27, 734–740.
- Qiang, Y., Zhang, S., Guo, L., Zheng, X., Xiang, B., Chen, S., 2017. Experimental and theoretical studies of four allyl imidazolium-based ionic liquids as green inhibitors for copper corrosion in sulfuric acid. *Corros. Sci.* 119, 68–78.
- Raghavachari, K., Binkley, J.S., Seeger, R., Pople, J.A., 1980. Self-Consistent Molecular Orbital Methods. 20. Basis set for correlated wave-functions. *J. Chem. Phys.* 72, 650–654.
- Rizvi, M., Gerengi, H., Kaya, S., Uygur, I., Yıldız, M., Sarioglu, I., Cingiz, Z., Mielniczek, M., El Ibrahimy, B., 2021. Sodium nitrite as a corrosion inhibitor of copper in simulated cooling water. *Sci. Rep.* 11 (1), 15847.
- Saad, A., Ech-chihbi, E., El-Hajjaji, F., Benhiba, F., Zarrouk, A., Kandri Rodi, Y., Taleb, M., El Biache, A., Rais, Z., 2021. Molecular dynamics, DFT and electrochemical to study the interfacial adsorption behavior of new imidazo[4,5-b] pyridine derivative as corrosion inhibitor in acid medium. *J. Appl. Electrochem.* 51, 245–265.
- Salim, R., Elaatioui, A., Benchat, N., Ech-chihbi, E., Rais, Z., Oudda, H., El Hajjaji, F., El Aoufir, Y., Taleb, M., 2017. Corrosion behavior of a smart inhibitor in hydrochloric Acid molar: Experimental and theoretical studies. *JMES* 8 (10), 3747–3758.
- Salim, R., Ech-chihbi, E., Oudda, H., El Hajjaji, F., Taleb, M., Jodeh, S., 2019. A review on the assessment of imidazole [1,2-a] pyridines as corrosion inhibitor of metals. *J. Bio Tribo. Corros.* 13, 5–11.
- Sastri, V.S., Perumareddi, J.R., 1997. Molecular Orbital Theoretical Studies of Some Organic Corrosion Inhibitors. *Corrosion* 53 (8), 617–622.
- Serdaroğlu, G., 2020. Harmine derivatives: a comprehensive quantum chemical investigation of the structural, electronic (FMO, NBO, and MEP), and spectroscopic (FT-IR and UV-Vis) properties. *Res. Chem. Intermediat.* 46, 961–982.
- Serdaroğlu, G., Kaya, S., Touir, R., 2020. Eco-friendly sodium gluconate and trisodium citrate inhibitors for low carbon steel in simulated cooling water system: Theoretical study and molecular dynamic simulations. *J. Mol. Liq.* 319, 114108.
- Singh, A., Ansari, K.R., Haque, J., Dohare, P., Lgaz, H., Salghi, R., Quraishi, M.A., 2018. Effect of electron donating functional groups on corrosion inhibition of mild steel in hydrochloric acid: Experimental and quantum chemical study. *J. Taiwan Inst. Chem. Eng.* 82, 233–251.
- Tana, B., Zhang, S., Liu, H., Qiang, Y., Li, W., Guo, L., Chen, S., 2019. Insights into the inhibition mechanism of three 5-phenyltetrazole derivatives for copper corrosion in sulfuric acid medium via experimental and DFT methods. *J. Taiwan. Inst. Chem. E.* 102, 424–437.
- Tomasi, J., Mennucci, B., Cammi, R., 2005. Quantum mechanical continuum solvation models. *Chem. Rev.* 105, 2999–3093.
- Verma, C., Ebenso, E.E., Quraishi, M.A., 2017. Ionic liquids as green and sustainable corrosion inhibitors for metals and alloys: An overview. *J. Mol. Liq.* 233, 403–414.
- Verma, C., Ebenso, E.E., Bahadur, I., Quraishi, M.A., 2018. An overview on plant extracts as environmental sustainable and green corrosion inhibitors for metals and alloys in aggressive corrosive media. *J. Mol. Liq.* 266, 577–590.
- Verma, C., Olasunkanmi, L.O., Bahadur, I., Lgaz, H., Quraishi, M.A., Haque, J., El-Sayed, M., Scherif, M., Ebenso, E.E., 2019. Experimental, density functional theory and molecular dynamics supported adsorption behavior of environmental benign imidazolium based ionic liquids on mild steel surface in acidic medium. *J. Mol. Liq.* 273, 1–15.
- Vinutha, M.R., Venkatesha, T.V., 2016. Review on Mechanistic Action of Inhibitors on Steel Corrosion in Acidic Media. *Port. Electrochim. Acta* 34 (3), 157–184.
- Zhang, M., Ettelaie, R., Yan, T., Zhang, S., Cheng, F., Binks, B.P., Yang, H., 2017. Ionic Liquid Droplet Microreactor for Catalysis Reactions Not at Equilibrium. *J. Am. Chem. Soc.* 139 (48), 17387–17396.
- Zhang, F., Tang, Y., Cao, Z., Jing, W., Wu, Z., Chen, Y., 2012. Performance and theoretical study on corrosion inhibition of 2-(4-pyridyl)-benzimidazole for mild steel in hydrochloric acid. *Corros. Sci.* 61, 1–9.